Calhoun: The NPS Institutional Archive

DSpace Repository

Theses and Dissertations | 1. Thesis and Dissertation Collection, all items

1989-06

The measurements of thermoacoustic phenomena using thermoacoustic couples

Ao, Chia-ning

Monterey, California. Naval Postgraduate School

http://hdl.handle.net/10945/27128

Downloaded from NPS Archive: Calhoun

http://www.nps.edu/library

Calhoun is the Naval Postgraduate School's public access digital repository for research materials and institutional publications created by the NPS community. Calhoun is named for Professor of Mathematics Guy K. Calhoun, NPS's first appointed -- and published -- scholarly author.

Dudley Knox Library / Naval Postgraduate School
411 Dyer Road / 1 University Circle
Monterey, California USA 93943

, CALIFORNIA 93943 5002

NAVAL POSTGRADUATE SCHOOL
Monterey, California

THESIS

A5673

The Measurements of Thermoacoustic Phenomena
Using Thermoacoustic Couples

by

Ao, Chia-ning

June 1989

Thesis Advisor: A. A. Atchley
Co-advisor: T. J. Hofler

Approved for public release; distribution unlimited.

T245587

Unclassified

ecurity Classification of this page

REPORT DOCUMENTATION PAGE

a Report Security Classification Unclassified	1b Restrictive Markings
a Security Classification Authority	3 Distribution Availability of Report
b Declassification/Downgrading Schedule	Approved for public release; distribution is unlimited.
Performing Organization Report Number(s)	5 Monitoring Organization Report Number(s)
a Name of Performing Organization: Naval Postgraduate School; 6b Office Symbol (If Applicable): 61	7a Name of Monitoring Organization: Naval Postgraduate School
c Address (city, state, and ZIP code): Monterey, CA 93943-5000	7b Address (city, state, and ZIP code): Monterey, CA 93943-5000
a Name of Funding/Sponsoring Organization; 8b Office Symbol (If Applicable)	9 Procurement Instrument Identification Number
c Address (city, state, and ZIP code)	10 Source of Funding Numbers: Program Element Number; Project No; Task No; Work Unit Accession No

1 Title (Include Security Classification) The Measurements of Thermoacoustic Phenomena Using Thermoacoustic Couples

2 Personal Author(s) Ao, Chia-ning

3a Type of Report	13b Time Covered	14 Date of Report (year, month,day)	15 Page Count
Master's Thesis	From To	June 1989	68

6 Supplementary Notation The views expressed in this thesis are those of the author and do not reflect the official olicy or position of the Department of Defense or the U.S. Government.

7 Cosati Codes			18 Subject Terms (continue on reverse if necessary and identify by block number)
ield	Group	Subgroup	Acoustics, Thermoacoustics, Thermoacoustic Heat Transport

9 Abstract (continue on reverse if necessary and identify by block number

Thermoacoustic heat transport and its applications, such as thermoacoustic engines and refrigerators, have een discussed in a number of articles over the past several years. However, lacking from these articles is a orough, quantitative experimental investigation of the basic theory underlying thermoacoustic heat transport. uch an investigation is the purpose of this thesis. A logical starting point for such a study is to investigate the implest class of thermoacoustic engine - a stack of short plates referred to as a ThermoAcoustic Couple, or TAC. he utility of this choice is that the theory can be reduced to its simplest form for analysis of the results. The esults of measurements of thermoacoustically generated temperature gradients in TACs subjected to acoustic tanding waves are reported. The value of the temperature gradient, which results from an acoustically generated ntropy flow in the gas in thermal contact with the plate, is a function of the acoustic pressure amplitude, the mean as pressure, the Prandtl number of the gas, the configuration of the TAC, and its position in the standing wave. Measurements were made with a computer controlled apparatus for drive ratios (the ratio of the acoustic pressure mplitude to the mean pressure of the gas) from approximately 0.1 to 2%, in argon and helium having mean ressures from approximately 0.1 to 0.3 MPa, for three different TACs as a function of their positions in the tanding wave. The results are compared with predictions based on a theory by Wheatley et al [J. Acoust. Soc. m. 74, 153-170 (1983)]. Three distinct regions of behavior are apparent over the range of drive ratios nvestigated. For drive ratios less than approximately 0.4%, there is overall good agreement between theory and neasurement. For drive ratios between approximately 0.4 and 1%, the agreement diminishes almost linearly with ncreasing drive ratio. For drive ratios greater than approximately 1%, irregularities appear in the temperature ifference data series and the discrepancy between theory and measurement generally remains approximately onstant, although some variations occur.

0 Distribution/Availability of Abstract	21 Abstract Security Classification	
[X] unclassified/unlimited [ ] same as report [ ] DTIC users	Unclassified	
2a Name of Responsible Individual: nthony A. Atchley	22b Telephone (Include Area code): (408) 646-2848	22c Office Symbol: Code 61Ay

D FORM 1473, 84 MAR 83 APR edition may be used until exhausted security classification of this page

All other editions are obsolete Unclassified

Approved for public release; distribution is unlimited.

The measurements of Thermoacoustic Phenomena Using Thermoacoustic Couples

by

Ao, Chia-ning
Lieutenant, Taiwan navy
B.S., Chinese Naval Academy on Taiwan, 1981

Submitted in partial fulfillment of the requirements for
the degree of

MASTER OF SCIENCE IN ENGINEERING ACOUSTICS

from the

NAVAL POSTGRADUATE SCHOOL
June 1989

ABSTRACT

Thermoacoustic heat transport and its applications, such as thermoacoustic engines and refrigerators, have been discussed in a number of articles over the past several years. However, lacking from these articles is a thorough, quantitative experimental investigation of the basic theory underlying thermoacoustic heat transport. Such an investigation is the purpose of this thesis. A logical starting point for such a study is to investigate the simplest class of thermoacoustic engine - a stack of short plates referred to as a ThermoAcoustic Couple, or TAC. The utility of this choice is that the theory can be reduced to its simplest form for analysis of the results. The results of measurements of thermoacoustically generated temperature gradients in TACs subjected to acoustic standing waves are reported. The value of the temperature gradient, which results from an acoustically generated entropy flow in the gas in thermal contact with the plate, is a function of the acoustic pressure amplitude, the mean gas pressure, the Prandtl number of the gas, the configuration of the TAC, and its position in the standing wave. Measurements were made with a computer controlled apparatus for drive ratios (the ratio of the acoustic pressure amplitude to the mean pressure of the gas) from approximately 0.1 to 2%, in argon and helium having mean pressures from approximately 0.1 to 0.3 MPa, for three different TACs as a function of their positions in the standing wave. The results are compared with predictions based on a theory by Wheatley et al [J. Acoust. Soc. Am. 74, 153-170 (1983)]. Three distinct regions of behavior are apparent over the range of drive ratios investigated. For drive ratios less than approximately 0.4%, there is overall good agreement between theory and

C.1

measurement. For drive ratios between approximately 0.4 and 1%, the agreement diminishes almost linearly with increasing drive ratio. For drive ratios greater than approximately 1%, irregularities appear in the temperature difference data series and the discrepancy between theory and measurement generally remains approximately constant, although some variations occur.

TABLE OF CONTENTS

I. INTRODUCTION 1

II. THEORY 4

A. INTRODUCTION 4

B. THERMOACOUSTIC EFFECT 4

III. EXPERIMENTAL APPARATUS AND PROCEDURE 22

A. INTRODUCTION 22

B. EXPERIMENTAL APPARATUS 22

1. Thermoacoustic Couples (TACs) 22

2. TAC Probe 26

3. Resonator Tube and Acoustic Driver Housing 29

4. TAC Positioning System 33

5. Electronic Instrumentation 35

C. EXPERIMENTAL PROCEDURE 38

IV. RESULTS AND DISUCSSION 40

A. INTRODUCTION 40

B. RESULTS AND DISCUSSION 40

V. SUMMARY, CONCLUSIONS, AND FUTURE WORK 55

A. SUMMARY 55

B. CONCLUSIONS 56

C. FUTURE WORK 57

LIST OF REFERENCES 58

INITIAL DISTRIBUTION LIST 59

ACKNOWLEDGEMENT

I thank almighty God who gave me such an amazing opportunity to observe the wonderful thermoacoustic phenomena of His creation. I also thank Him for the opportunity to work with my thesis advisor, Dr. Anthony A. Atchley, and co-advisor, Dr. Thomas J. Hofler.

I would like to express my gratitude to my advisors for their encouragement and help while working on my thesis. Through their constant interest and enthusiasm they have taught me many brand new ideas, I have learned not only about science and the laboratory but also a great deal about patience and faith.

Another gift from God is the help from George Jaksha and Steven Blankschein of the physics department machine shop, without whom the experimental apparatus would never have been built.

May God bless them all and let them keep sharing their love with others.

I. INTRODUCTION

Thermoacoustic heat transport, the thermoacoustic engine, and its applications have been discussed in a number of articles over the past several years [Ref. 1—6]. Lacking from these articles is a thorough, quantitative experimental investigation of the basic theory underlying thermoacoustic heat transport. A logical starting point for such a study is to investigate the simplest class of thermoacoustic engine — a stack of short plates referred to as a ThermoAcousticCouple, or TAC. The utility of this choice is that the theory can be reduced to its simplest form for analysis of the results. The purpose of this thesis is to report the results of a set of measurements on such an engine, along with a quantitative comparison with theory.

The first measurements of the thermoacoustic effect using a TAC were performed by Wheatley, et al.[Ref. 1—3] They measured the temperature difference developed across a TAC as a function of its position in an acoustic standing wave. At relatively low values of the drive ratio (the ratio of the acoustic pressure amplitude to the mean pressure of the gas), the temperature difference across the TAC is a nearly sinusoidal function of its position in the standing wave. The zeros in the temperature difference occur at both pressure and velocity nodes (or antinodes); and, the hot end of the TAC is always closer to the nearest pressure antinode. Although they developed a theoretical expression for the temperature difference [Ref. 6], Wheatley, et al attempted little quantitative comparison of their results with theory. As they state, the purpose of their measurements was only to give them confidence that they understood the general features of thermoacoustic heat transport, before exploring more complex

engines. Their quantitative comparisons were limited to a single region in the standing wave (near a pressure node) and to low values of the drive ratio.

All of Wheatley et al's published results were made at nearly equal values of the drive ratio, the value being approximately 3×10^{-3}. However, they did discuss the effect of increasing the drive ratio. As the drive ratio "increases, the [temperature difference] changes from the nearly perfect sinusoid . . . to something closer to a sawtooth shape, with the maxima (minima) shifted to be near the pressure antinodes. There are still zeros at velocity and pressure antinodes, but the slope of the curve is very steep and negative at the pressure antinodes [Ref. 2]. They go on to provide a theoretical explanation for this behavior.

In light of this previous work, we have undertaken a quantitative investigation of thermoacoustic heat transport. The results of the initial phase of this work are reported here. In particular, we have measured the temperature difference developed across short stacks of plates in acoustic standing waves as a function of the position of the plates in the acoustic field, the drive ratio, the plate configuration, the thermal properties of the plates, and the thermophysical properties of the gas. The specific aim of these measurements is to first verify the theory developed by Wheatley et al by comparing it to measured results at low drive ratios. Secondly, the comparisons will be extended to high drive ratios. These latter comparisons are especially interesting, because commercially useful thermoacoustic devices will likely operate at high drive ratios.

The thermoacoustic effect is described in the next chapter, along with a discussion of Wheatley's et al equation for the temperature difference developed across a TAC, which will be used to analyze the results of our measurements. A

description of the experimental apparatus and the procedure for making the measurements are explained in Chapter III. The results of the measurements are analyzed in Chapter IV. The final chapter contains a summary of the thesis and recommendations for future work.

II. THEORY

A. INTRODUCTION

The stack of plates is a rather simple structure, which may function either as a prime mover (a motor producing work), or as a heat pump (e.g. a refrigerator). This chapter is organized as follows: first, a description of the thermoacoustic effect in a thermally driven oscillator (prime mover) is given and, second, the operation of a thermoacoustic heat pump is described. Basically, a large temperature gradient imposed on the stack of plates will generate an acoustic standing wave, with the thermal energy stored in the plates being transferred to the energy of the standing wave. The operation of the heat pump is the functional reverse of the prime mover. An acoustic standing wave imposed on a stack of plates will cause a temperature gradient to develop, with the acoustic energy being transferred to the thermal energy of the plates. After this discussion an equation for the temperature difference across the plates, ΔT, will be introduced which was obtained from Wheatley [Ref. 2 Eq.17].

B. THERMOACOUSTIC EFFECT

Each plate is assumed to have a sufficiently large temperature gradient, ∇T, across it with no heat conduction in the longitudinal (wave propagation) direction. Consider a small parcel of gas located one thermal penetration depth from a plate and initially having the same temperature, T_m, as the portion of the plate adjacent to it. When ∇T is large enough, this gas parcel will spontaneously oscillate at the resonance frequency of the acoustic system. The plates act as a source of

energy that generates the acoustic standing wave. Thus the plates function as a *prime mover*, generating acoustic work. The functional diagram of the prime mover is shown in Fig. 1.

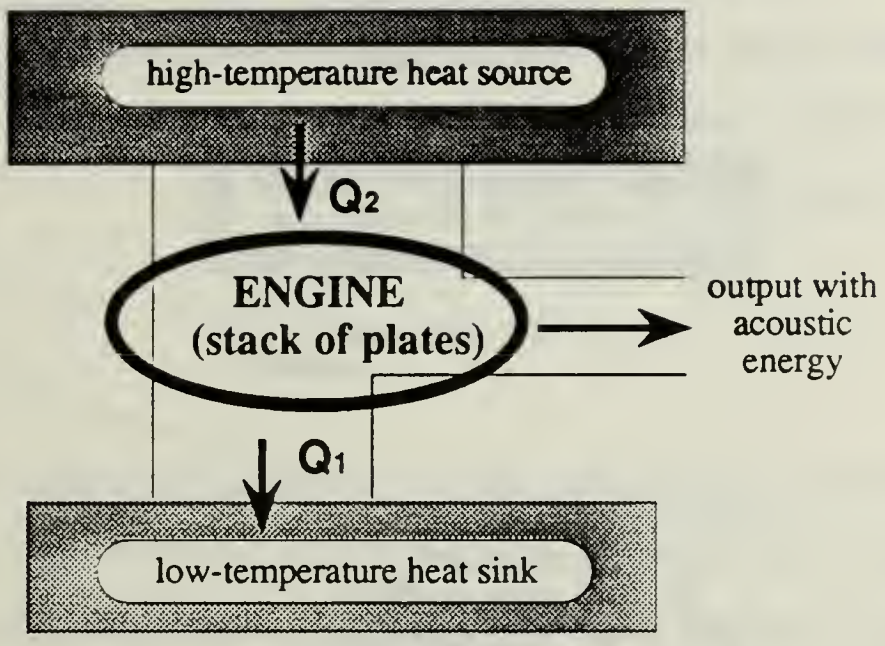

Fig. 1 Prime mover ($\Gamma>1$; $\Gamma = \frac{\nabla T}{\nabla T_{crit}}$)

The function of the prime mover may be simply described by the following table :

(1)	A stack of plates must be installed in the resonator and the material of those plates should be of low thermal conductivity.
(2)	The temperature gradient in the stack should be sufficiently large and oriented such that the cooler end of the stack is adjacent to a velocity antinode of the standing wave and the hotter end adjacent to a pressure antinode.

Table 1

Next, the functional reverse of the preceding phenomena is considered. Assume there is no temperature gradient in the stack. Acoustic energy is supplied to the resonator by a source operating at a frequency corresponding to a resonant mode. A simple duct with a stack of plates is illustrated in Fig. 2. There will be as many plates in parallel as possible, consistent with optimum efficiency. The plate length is short compared with both the resonant tube and the radian length of the acoustic wave λ, where $\lambda = \frac{\lambda}{2\pi} = \frac{1}{k}$

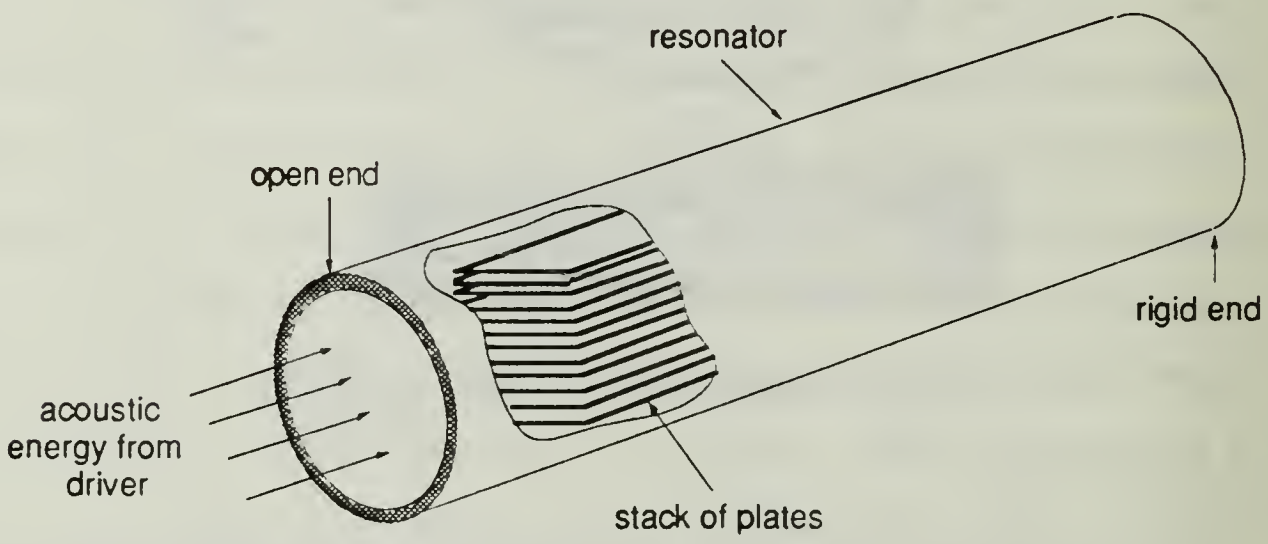

Fig. 2 A simplified illustration of the resonator and stack.

The gas parcels will oscillate with the driving frequency and transport heat from one end of the plate to the other and eventually establish a temperature gradient. A functional diagram of the heat pump is shown in Fig. 3.

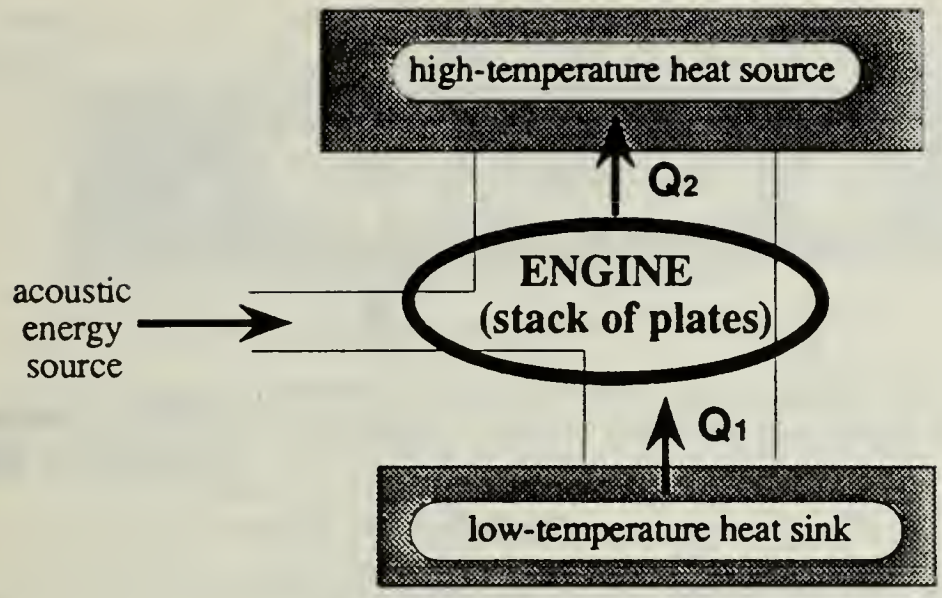

Fig. 3 Heat pump ($\Gamma<1$)

In order to understand this effect, the heat pumping cycle between a single plate and a gas parcel may be observed in microscopic view. For ease of description, we will assume an articulated motion of the parcel rather than a sinusoidal motion, and all viscous effects are neglected. The four stages of the heat exchanging cycle are illustrated in Fig. 4(a) and 4(b).

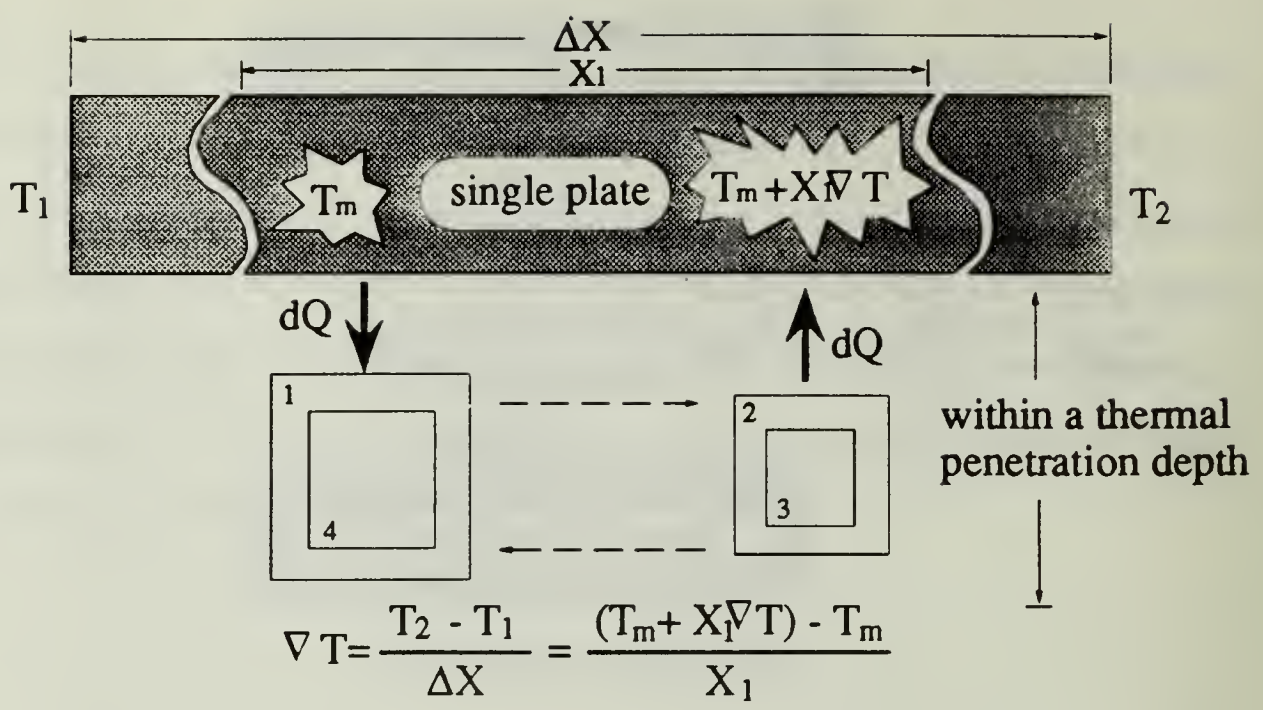

Fig. 4(a) Microscopic view of the heat exchange between the single plate and the gas particle

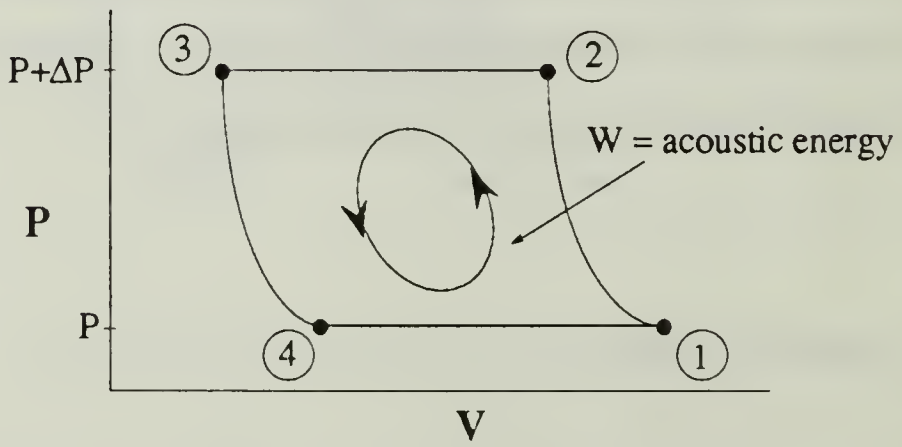

Fig. 4(b) P-V diagram of the cycle is half heat-exchange & half without heat exchange

The phenomena occurring in a complete cycle are listed in Table 2.

Process	Description of the Phenomena
$1 \rightarrow 2$	(a) The acoustic energy is supplied to the resonant tube and the gas parcel is excited and displaced toward the pressure antinode by an amount X_1. (b) The compression process is adiabatic. (c) The pressure increases from P to $P+\Delta P$. (d) The temperature increases from T_m to T_m+T'
$2 \rightarrow 3$	(a) An amount of heat dQ flows from the gas parcel to the plate (b) The heat exchange process is isobaric. (c) The pressure is unchanged. (d) The temperature decreases from T_m+T' to $T_m+T'-\delta T$
$3 \rightarrow 4$	(a) The gas parcel is displaced back toward the pressure node by an amount X_1. (b) The expansion process is adiabatic. (c) The pressure decreases from $P+\Delta P$ to P. (d) The temperature decreases from $T_m+T'-\delta T$ to $T_m-\delta T$
$4 \rightarrow 1$	(a) An amount of heat dQ flows from the plate to the gas parcel (b) The heat exchange process is isobaric. (c) The pressure is unchanged. (d) The temperature increases from $T_m-\delta T$ to T_m

Table 2

δT is the temperature change in the gas due to the heat flow process and T' is the temperature change in gas due to the adiabatic compression or expansion process. The heat flow dQ is proportional to the temperature difference between the gas parcel and the portion of the plate adjacent to the parcel, during the heat exchange parts of the cycle. For example, the temperature of the plate at a point may be $T_m+X_1\nabla T$ and the temperature of the gas parcel is T_m+T'. Then the heat flux dQ is

$$dQ \propto \Delta T$$

and

$$\Delta T = - [T_{plate} - T_{gas}]$$

$$= - [(T_m + X_1 \nabla T) - (T_m + T')]$$

$$= T' - X_1 \nabla T$$

$$= T'(1 - \frac{\nabla T}{\frac{T'}{X_1}})$$

$$= T'(1 - \frac{\nabla T}{\nabla T_{crit}})$$

$$= T'(1 - \Gamma) \qquad \text{Eq.(1)}$$

where

$$T' = \frac{T_m \beta}{\rho_m c_p} P_1 \qquad \text{[Ref. 2 Eq.4]} \qquad \text{Eq.(2)}$$

and

T_m = mean absolute temperature;

β = isobaric expansion coefficient

C_p = specific heat of constant gas pressure

ρ_m = density of gas

P_1 = acoustic pressure amplitude (or the adiabatic pressure change)

For an ideal gas the product $T_m\beta$ equals unity.

The value for ∇T which makes $\Delta T=0$ in Eq.(1) is known as the critical gradient so that,

$$\Gamma = \frac{\nabla T}{\nabla T_{crit}} \qquad \text{Eq.(3)}$$

and ∇T_{crit} is the maximum temperature gradient that can be acoustically induced on to this plate i.e.

$$\nabla T_{crit} = \frac{T'}{X_1} \qquad \text{Eq.(4)}$$

It is the boundary between the heat pump and prime mover.

The result after each cycle is that the gas parcel has transferred a small amount of heat dQ over a short distance X_1. The deposited heat is picked up by an adjacent parcel and moved still further during the subsequent cycles. The heat is shuttled down the plate, toward the pressure antinode until it reaches the end of the plate. It collects there until it is conducted back through the plate and the surrounding gas.

When the cycle operates continuously, it will heat up or cool down the tube on either side of the stack. That is, the rigid end (pressure antinode and velocity node) will be heated up and the other end will be cooled down. The stack acts as a *heat engine* of the *heat pump* type. The requirements for the refrigeration phenomena are listed in the following table:

(1) A stack of plates must be installed in the resonator and the material of each plate should be of low thermal conductivity.
(2) Initially, $\nabla T=0$ and acoustic energy is supplied to the resonator.
(3) Because of the acoustic resonance, the temperature gradient (∇T) will increase, so that one end of the resonator will become colder and the other end will become hotter.

Table 3

The entropy flow (ΔS) occuring in a complete cycle are listed as follows:

Process	Description of the Phenomena
$1 \rightarrow 2$	(1) Adiabatic compression process (2) $S_1=S_2$; $\Delta S=0$
$2 \rightarrow 3$	(1) Isobaric heat exchange process (2) $\Delta S= S_3 - S_2 = \frac{-dQ}{T_m+T-\delta T}$ (3) The right side of the plate gains entropy ΔS
$3 \rightarrow 4$	(1) Adiabatic expansion process (2) $S_1= S_2$; $\Delta S=0$
$4 \rightarrow 1$	(1) Isobaric heat exchange process (2) $\Delta S= S_1 - S_4= \frac{+dQ}{T_m-\delta T}$ (3) The left side of the plate loses entropy ΔS.

Table 4

The result after each cycle is that the left and right portions of the plate, located at the extreme position of parcel motion, will have an entropy difference of at least $2\Delta S$. During a single cycle, entropy is transferred by the isobaric process $2 \rightarrow 3$ and $4 \rightarrow 1$. The entropy increment per unit mass from left to right is then approximated by [Ref. 2 Eq.14a]

$$\Delta S \propto \frac{c_p}{T_m} T(\Gamma-1) = \frac{c_p}{T_m} \frac{T_m \beta}{\rho_m c_p} P_1(\Gamma-1) \qquad \text{Eq.(5)}$$

And the steady entropy flow is

$S = \rho_m V \Delta S$, where V is the volume velocity.

The configuration in Fig. 5 shows a solid plate with length ΔX, width $\frac{\Pi}{2}$ and negligible thickness. The length ΔX is aligned along the x-axis and an ordinary acoustic standing wave is directed along X in the gas around the plate. The only way that the heat can be transported along X is by the hydrodynamic transport of entropy, carried by the oscillatory velocity u_1. In the Y direction, the heat-flux density is the largest at about a distance δ_κ from the surface of the plate. We have defined the plate width as $\frac{\Pi}{2}$ because a cross-section perpendicular to X through the plate reveals a perimeter Π. Then the cross-sectional area for heat flux along X is $\Pi\delta_\kappa$.

i.e. $(\frac{\Pi}{2} * \delta_\kappa)_{top} + (\frac{\Pi}{2} * \delta_\kappa)_{bottom} = \Pi\delta_\kappa$ [Ref. 6 p.17 Fig. 9]

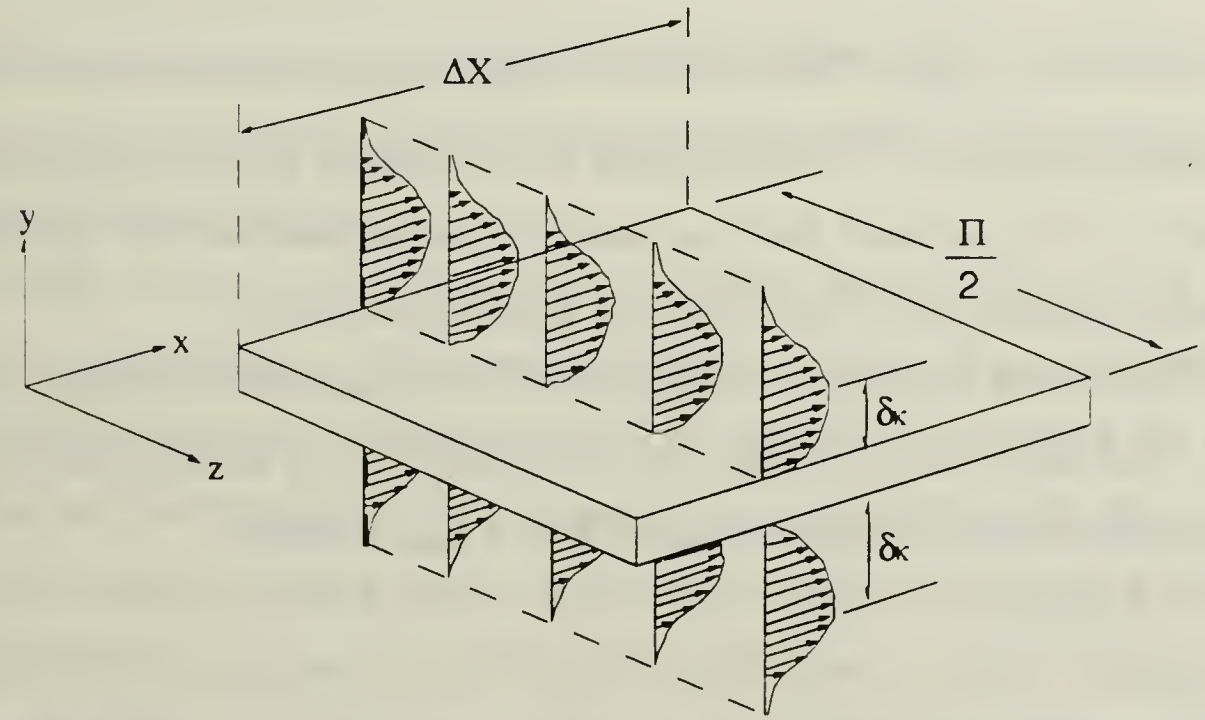

Fig. 5 Thermal penetration depth of the gas around the plate [Ref. 6 P.11 and Fig. 9]

The thermodynamically active volume velocity is $V \propto \prod \delta_\kappa u_1$ Eq.(6)

where u_1 is the acoustic particle velocity.

According to the definition of the entropy :

$$\delta S = \frac{\delta Q}{T_m} \qquad \text{Eq.(7)}$$

we then have

$$\delta Q = \delta S T_m = \rho_m V \Delta S T_m \propto -\rho_m \prod \delta_\kappa u_1 \quad \frac{c_p}{T_m} \frac{T_m \beta}{\rho_m c_p} P_1 (\Gamma - 1) T_m$$

$$= -\prod \delta_\kappa T_m \beta p_1 u_1 (\Gamma - 1)$$

[Ref. 2 Eq.15] Eq.(8)

The term $\frac{T_m \beta}{\rho_m c_p}$ determines the adiabatic temperature change per unit pressure change and $\prod \delta_\kappa$ is the volume of the gas-plate thermal interaction. The quantity $(\Gamma - 1)$ indicates how the entropy flow depends on the temperature gradient and that when $\nabla T = \nabla T_{crit}$, the entropy flow is zero.

The total heat flux Q is proportional to $\prod$ but independent of the plate length ΔX. The temperature difference ΔT is correlated to the acoustic pressure and gas parcel velocity. In the case when $\nabla T << \nabla T_{crit}$, we have

$$\Delta T \propto p_1 u_1$$

and

$$p_1 = p_0 \cos(kx)\, e^{j\omega t} \qquad \text{[Ref. 6 Eq.10]}$$

$$u_1 = u_0 \sin(kx)\, e^{j\omega t} \qquad \text{Eq.(9)}$$

where k is the wave number, x is the displacement from the closed end of the tube and p_0 , u_0 are the magnitude of the pressure and velocity respectively.

At the rigid end (i.e. at x=0), p_1 has the maximum value while u_1 has the minimum value. They are 90° out of phase with respect to each other. Ignoring the time dependence term $e^{j\omega t}$ in p_1 and u_1 and multiplying them together gives,

$$p_1 u_1 = p_0 u_0 \cos(kx) \sin(kx) = p_0 u_0 \frac{1}{2} \sin(2kx) \qquad \text{Eq.(10)}$$

$$\therefore \Delta T \propto p_0 u_0 \sin(2kx) \qquad \text{Eq.(11)}$$

and the temperature gradient of whole section of the TAC length (ΔX) will be:

$$\nabla T = \frac{\Delta T}{\Delta X} \qquad \text{Eq.(12)}$$

At either a pressure node or a velocity node ΔT will be zero. The relationship among the acoustic pressure, particle velocity and the temperature difference is graphically shown in Fig. 6.

Consider the fact that the heat flow is always in the direction towards the nearest pressure antinode. This is expected since, as a parcel of gas is moved in the direction towards a pressure antinode, the parcel is compressed and its resulting increased temperature will cause heat to be transferred to the plate. If the parcel is moved toward a pressure node, it will expand and its resulting lower temperature will cause heat to be removed from the plate. In order to measure ΔT on the plates, a thermopile is laminated in the central plate, and the whole stack is called a "*thermoacoustic couple*" or "TAC".

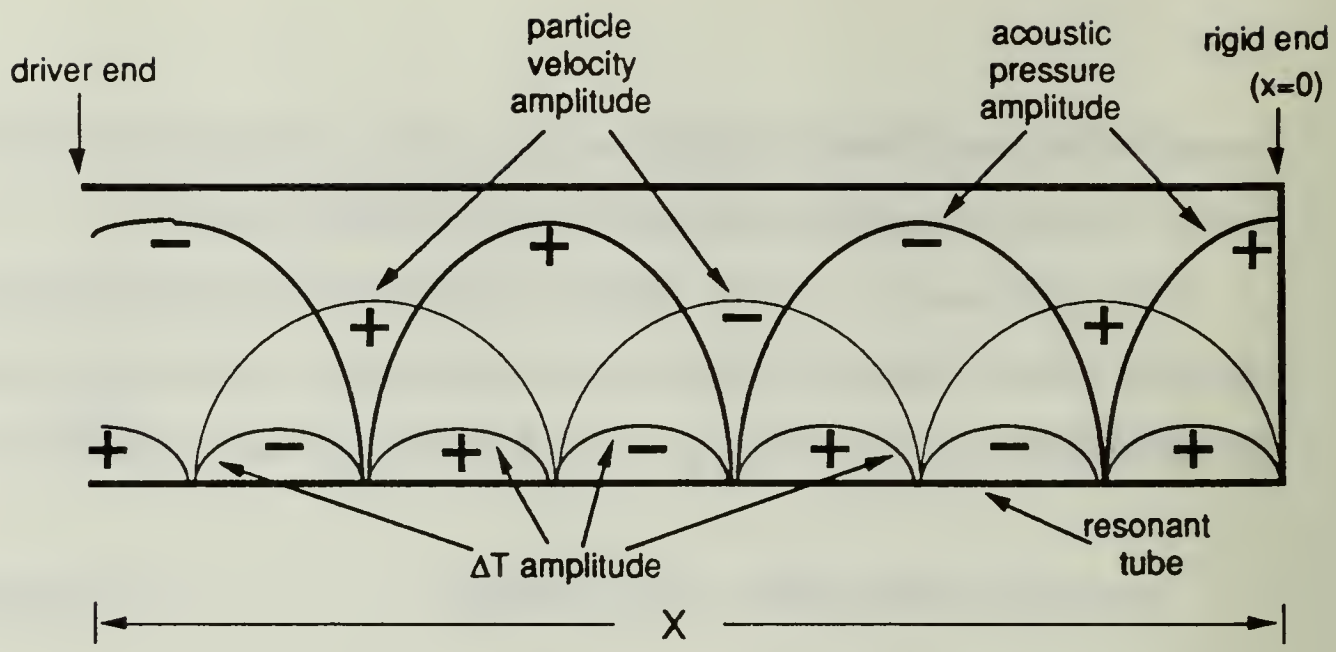

Fig. 6 The amplitude distribution of p_1 ,u_1 and ΔT in the resonant tube and their phased are assigned by $\pm$ sign.

Aside from the heat flux, the work flux, i.e. the acoustic power, is also important. Ignoring the viscosity, the acoustic work w is given by the area of the p-v diagram of Fig. 4(b).

$$w = P\,dV \qquad \text{Eq. (13)}$$

The total acoustic power W dissipated by the plate can be calculate by integrating over all the gas parcels dxdydz along the plate.

$$W = \frac{1}{4}\Pi\delta_k\Delta X\,\frac{T_m\beta^2\omega}{\rho_m c_p}P_1^2(\Gamma\text{-}1) \qquad \text{[Ref. 6 Eq.37]} \quad \text{Eq.(14)}$$

So the acoustic power is proportional to the plate length ΔX and the total energy flow H is then the sum of work flow and heat flow.

$$H = Q + W \qquad \text{Eq.(15)}$$

At the rigid end, the pressure is a maximum (called *pressure antinode*) and at the open end where there is a pressure release, the pressure is a minimum (called a *pressure node*). A common term (Γ-1) exists in both equations for Q and W given in Eq.(7) and (14).

When $\Gamma<1$ (or when $\nabla T<\nabla T_{crit}$), then Q is positive and the heat flux is directed toward the pressure antinode so the open end will become cooler and the closed end will become hotter. In this case, the acoustic power W is dissipated by the gas parcels near the plates. The plates function as a heat pump. This is illustrated in Fig. 7, for which

$$\Delta T = T_2 - T_1 = T_{hot} - T_{cold} \qquad \text{Eq.(16)}$$

is obviously a positive value. This may be proved by the measurement of ΔT. A positive half cycle appears when the TAC is moving away from a pressure antinode, as shown in Fig. 20.

The prime mover functions as follows: When $\Gamma>1$ (or when $\nabla T>\nabla T_{crit}$), then Q is negative and the heat flux is directed toward the pressure node. This tends to make the hot closed end less hot and the cold open end less cold. In this case, acoustic power W is generated by the gas parcels near the plates. The plates function as a prime mover. This is illustrated in Fig. 8, for which

$$\Delta T = T_2 - T_1 = T_{cold} - T_{hot} \qquad \text{Eq.(17)}$$

is obviously a negative value.

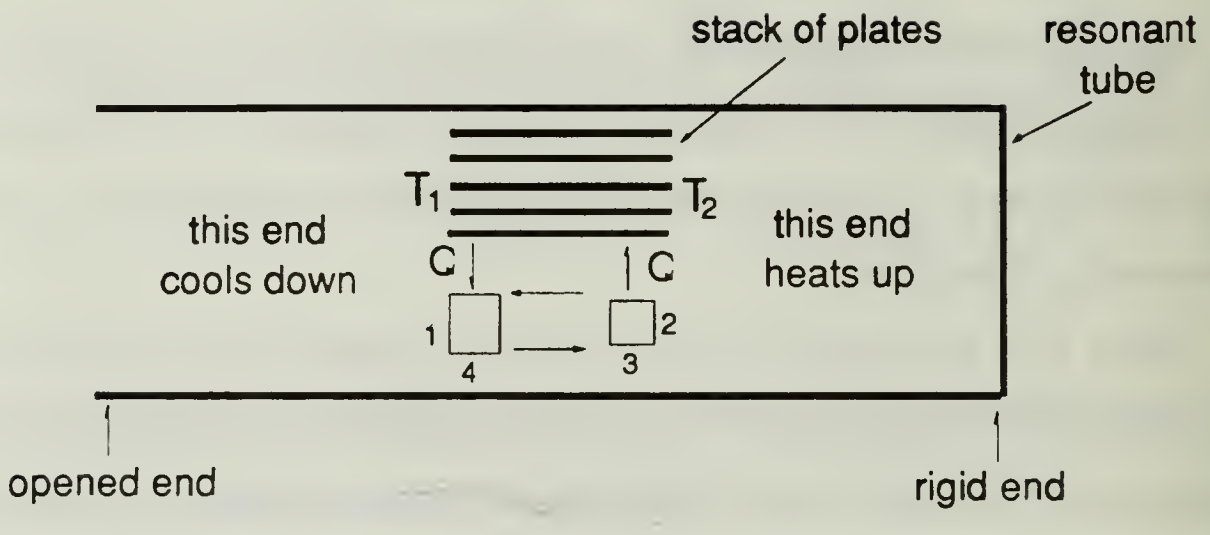

Fig. 7 When $\Gamma<1$, the TAC is a heat pump.

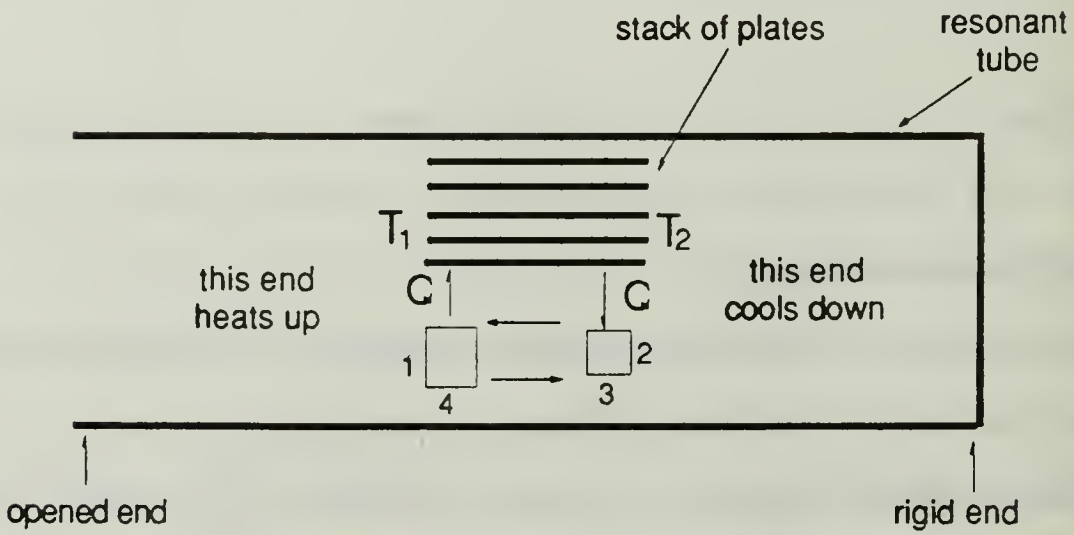

Fig. 8 when $\Gamma>1$, the TAC is a prime mover

When $\Gamma=1$ (or when $\nabla T=\nabla T_{crit}$), no heat transfer takes place. The gas parcel is compressed and expanded causing its temperature to increase and decrease as it moves. With this temperature gradient in the plate, there is no temperature difference between the parcel and the portion of the plate adjacent to it.

In our investigation, there are no temperature gradients in the beginning. When $\Gamma=0$, the heat flow initially has a large positive value. This causes the temperature gradient across the plate to increase toward the value of ∇T_{crit}. However, there is a return heat flow Q_r caused by this gradient and the thermal conductivity of the plate material, which is given by:

$$Q_r = \kappa A \nabla T \qquad \text{Eq.(18)}$$

So the net heat flow of the whole system Q_{net} will be

$$Q_{net} = Q - Q_r \qquad \text{Eq.(19)}$$
$$= \prod \delta_\kappa T_m \beta p_1 u_1 (1-\Gamma) - \kappa A \nabla T$$

At steady state, $Q = Q_r$, and $Q_{net} = 0$, so ∇T will increase only until a steady state is achieved.

The equation for temperature difference across the TAC, derived by Wheatley [Ref. 6 Eq.17] , is :

$$\Delta T = \frac{\dfrac{\frac{1}{4} P_0^2 \delta_\kappa (1+\sigma^{1/2})}{(\rho_m c (\frac{\kappa d_2}{\Delta X})(1+\sigma))} \sin(\frac{2\omega x}{c})}{\dfrac{(1+P_0^2 \delta_\kappa (1-\sigma^{3/2}))}{(4(\frac{\kappa d_2}{\Delta X})\rho_m \Delta X (\gamma-1)(1-\sigma^2))} (1-\cos(\frac{2\omega x}{c}))}$$

Eq.(20)

where

ΔT = temperature difference across the plate

P_0 = peak acoustic pressure of the driver

δ_κ = thermal penetration depth

σ = Prandtl number of the gas

γ = specific heat ratio of the gas $(= \frac{C_p}{C_v})$

ΔX = plate length

T_m = mean ambient temperature

ρ_m = mean density of the gas [Ref. 7]

c = sound velocity in the gas

ω = angular frequency

x = TAC center position measured from the closed end of the tube

κ = thermal conductivity

d_2 = thickness of the plate

The term κd_2 will be a function of the properties of the gas and the plate. For example, if a G-10 fiber glass and stainless steel laminated plate is used, then the term κd_2 will be

$$\kappa d_2 = \kappa_{gas} d_{gas} + \kappa_{fg} d_{fg} + \kappa_{ss} d_{ss} + \kappa_{gas} d_{gas} \quad \text{Eq.(21)}$$

$$= \kappa_{fg} d_{fg} + \kappa_{ss} d_{ss} + \kappa_{gas} * (\text{spacing})$$

Since the gas path on each side of the plate is one half of the plate separation, the $\kappa_{gas} d_{gas}$ term appears twice. This means the combination of the upper and lower side gas path thickness will be equal to a plate separation, i.e.

$$2 * d_{gas} = \text{the separation distance between two plates} \quad \text{Eq.(22)}$$

Measurements were made on a TAC that was mounted on a probe and moves along the resonant tube. The results will be compared to the theory given by Eq. (20).

III. EXPERIMENTAL APPARATUS AND PROCEDURE

A. INTRODUCTION

A description of the experimental apparatus is given in this chapter along with a discussion of the procedure followed during data acquisition. The discussion of the apparatus will be divided into the following sections: the TACs; the TAC probe and associated electrical wiring; the resonator tube and the acoustic driver housing; the TAC positioning system; and the electronic instrumentation. The experimental procedure is discussed in the final section.

B. EXPERIMENTAL APPARATUS

1. Thermoacoustic Couples (TACs)

Three TAC's were used in these measurements. A description of the individual TACs are given in Tables 5, 6, and 7. The plates of TAC #1 are G-10 fiberglass, while those of TACs #2 and #3 are a lamination of 302 stainless steel and G-10 fiberglass epoxied together. As shown in Fig. 9, each TAC consisted of a stack of five plates separated by approximately 1.5 mm. The center plate of each stack is a lamination of two plates. A thermopile, consisting of several thermocouple junctions in series, is located between these two plates. The thermopiles used on these TACs had either four or five junctions. The purpose of the thermopile is to provide more temperature difference measuring sensitivity. In order to determine the temperature difference developed across the TAC, the

thermopile output is measured. The measured voltage is divided by the number of thermocouples comprising the thermopile (N) and then divided by the sensitivity (in V/°C) of the particular type of thermocouple used. Type E, chromel-constantan, thermocouples are used in these measurements. Aside from the thermopile, a single thermocouple is mounted on the plate next to the center plate to allow measurement of the temperature of the TAC.

TAC#3	
Upper layer	• AISI-302 stainless steel • Size: 6.85 mm long * 25.3 mm wide * 0.0889 mm thick • Thermal conductivity : 11.8 $\frac{W}{mK}$ [Ref. 10]
Lower layer	• G-10 fiberglass • Size: 6.85 mm long * 25.3 mm wide * 0.1016 mm thick • Thermal conductivity : 0.48 $\frac{W}{mK}$
• Thermopile junction pairs number N=5	
• Thermocouple wire diameter : 0.0254 mm (0.001")	
• Number of plates : 5	
•Thickness of the TAC : 8.15 mm	
• Spacing in between any two adjacent plates : 1.52 mm	

Table 5 The specification of the TAC#3

TAC#2	
Upper layer	• AISI-302 stainless steel • Size: 6.8 mm long * 25.3 mm wide * 0.0889 mm thick • Thermal conductivity : 11.8 $\frac{W}{mK}$ [Ref. 10]
Lower layer	• G-10 fiberglass • Size: 6.8 mm long * 25.3 mm wide * 0.1778 mm thick • Thermal conductivity : 0.48 $\frac{W}{mK}$
• Thermopile junction pairs number N=5	
• Thermocouple wire diameter : 0.0762 mm (0.003")	
• Number of plates : 5	
•Thickness of the TAC : 7.7 mm	
• Spacing in between any two adjacent plates : 1.52 mm	

Table 6 The specification of the TAC#2

TAC#1	
Upper layer	• G-10 fiberglass • Size: 10 mm long * 25.4 mm wide * 0.33 mm thick • Thermal conductivity : 0.48 $\frac{W}{mK}$
Lower layer	• The same G-10 fiberglass as the upper layer
• Thermopile junction pairs number N=4	
• Number of plates : 5	
•Thickness of the TAC : 8.15 mm	
• Spacing in between any two adjacent plates :1.53 mm	

Table 7 The specification of the TAC#1

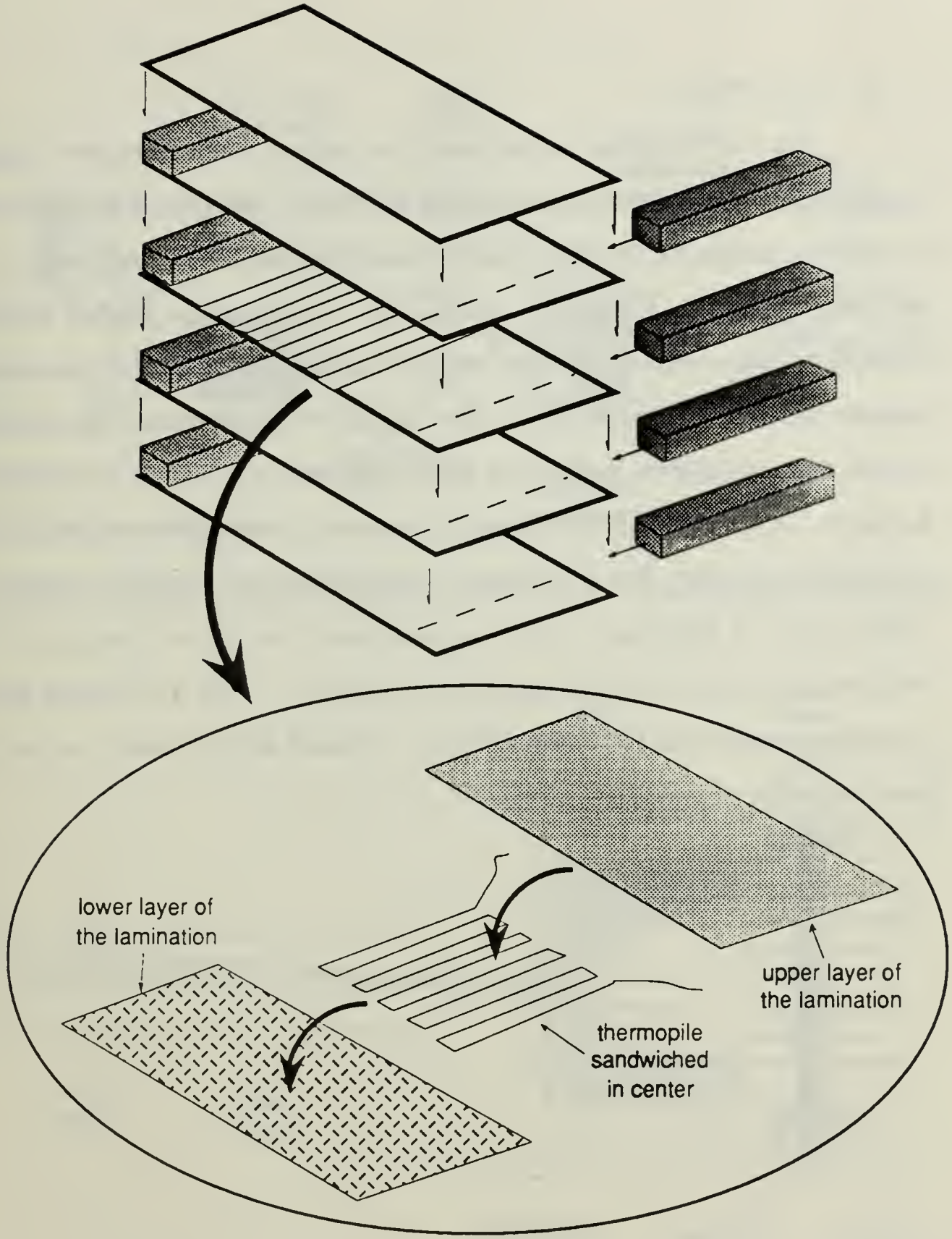

Fig. 9 The structure of the TAC and the enlarged view of the central plate lamination

2. TAC Probe

The TAC must be moved along the axis of a resonant tube in these measurements. In order to accomplish this positioning, the TAC is mounted on to the end of a hollow 1/8 inch OD stainless steel tube, called the TAC probe. The mounting bracket is illustrated in Fig. 10. An Endevco Model 8550m1 microphone is also mounted on this bracket to allow measurement of the acoustic pressure experienced by the TAC. The various wires associated with the TAC and the microphone pass through the hollow tube and exit into the tail section of the probe. A pressure tight feedthrough connector is connected to the probe tube via Swagelok fittings. The feedthrough allows for external electrical connections without loss of pressure in the resonator tube and driver housing. The feedthrough connector is illustrated in Figs. 11 and 12. The TAC probe passes through a pressure tight O-ring connector located in the closed end of the resonator tube.

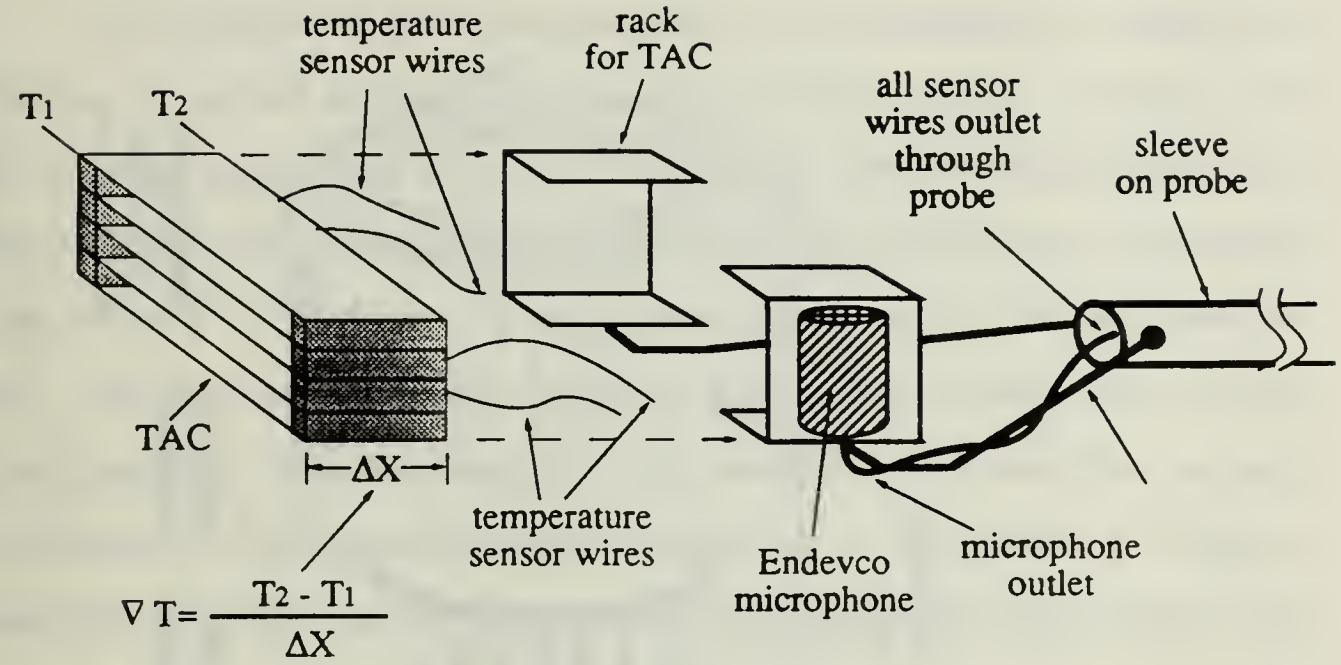

Fig. 10 The structure relationship of the TAC, microphone and probe

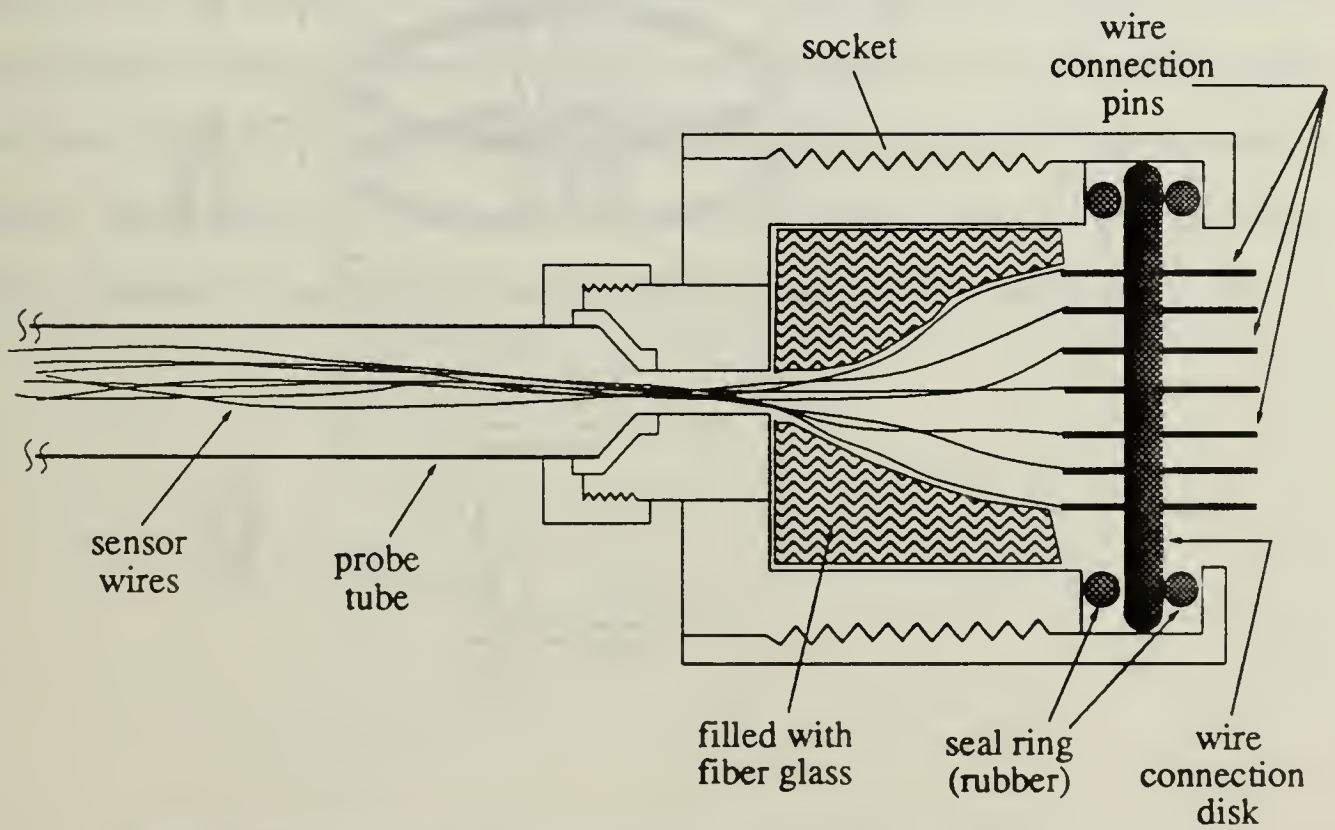

Fig. 11 The anatomy view of the probe tail portion

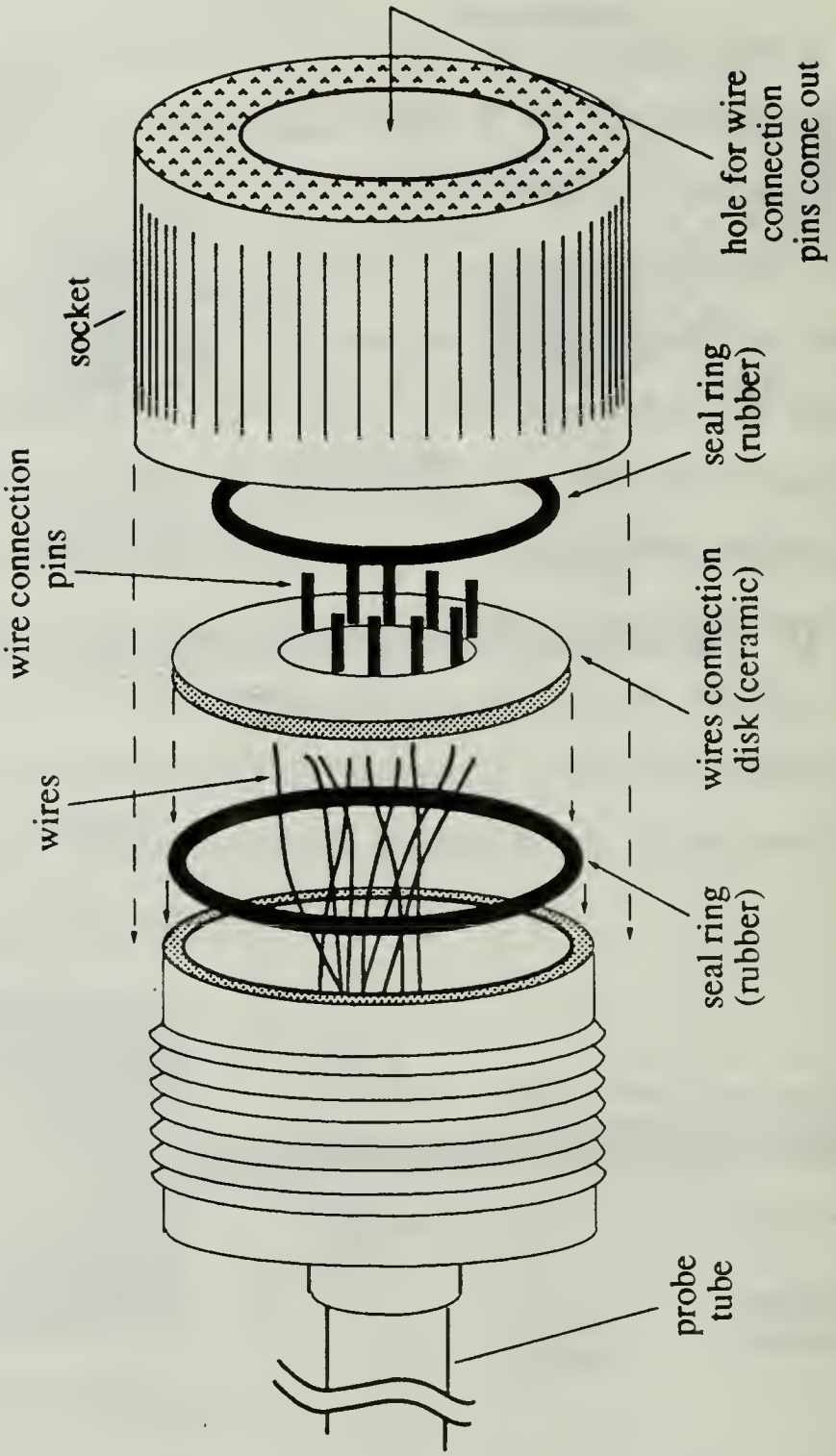

Fig. 12 The structure of the probe tail portion

3. Resonator Tube and Acoustic Driver Housing

The purpose of these measurements is to investigate the temperature difference developed across a TAC located within an acoustic standing wave. The standing wave is set up with a JBL Model—2445J compression driver located within a pressure housing. The driver housing is bolted via a brass flange to the end of a 1.217 m long 3.8 cm diameter copper tube, called the resonator tube. The other end of the resonator tube is also flanged. A brass plate is bolted to this flange and forms the closed end of the resonator. This brass plate contains the connector through which the probe tube passes. It also houses an Endevco Model 8510B-5 high intensity pressure transducer, which is used to monitor the acoustic pressure at the closed end. The entire length of the resonator is surrounded by a 7.6 cm diameter brass tube. Water is circulated, with a Neslab Model RTE-110 circulation temperature control bath, through the region between the two tubes in order to maintain a uniform temperature along the resonator tube. The water is also circulated around the driver housing through flexible plastic tubing. The resonator and driver housing are illustrated in Figs. 13 and 14. The TAC is centered in the resonator with a spring-loaded tripod pictured in Fig. 15.

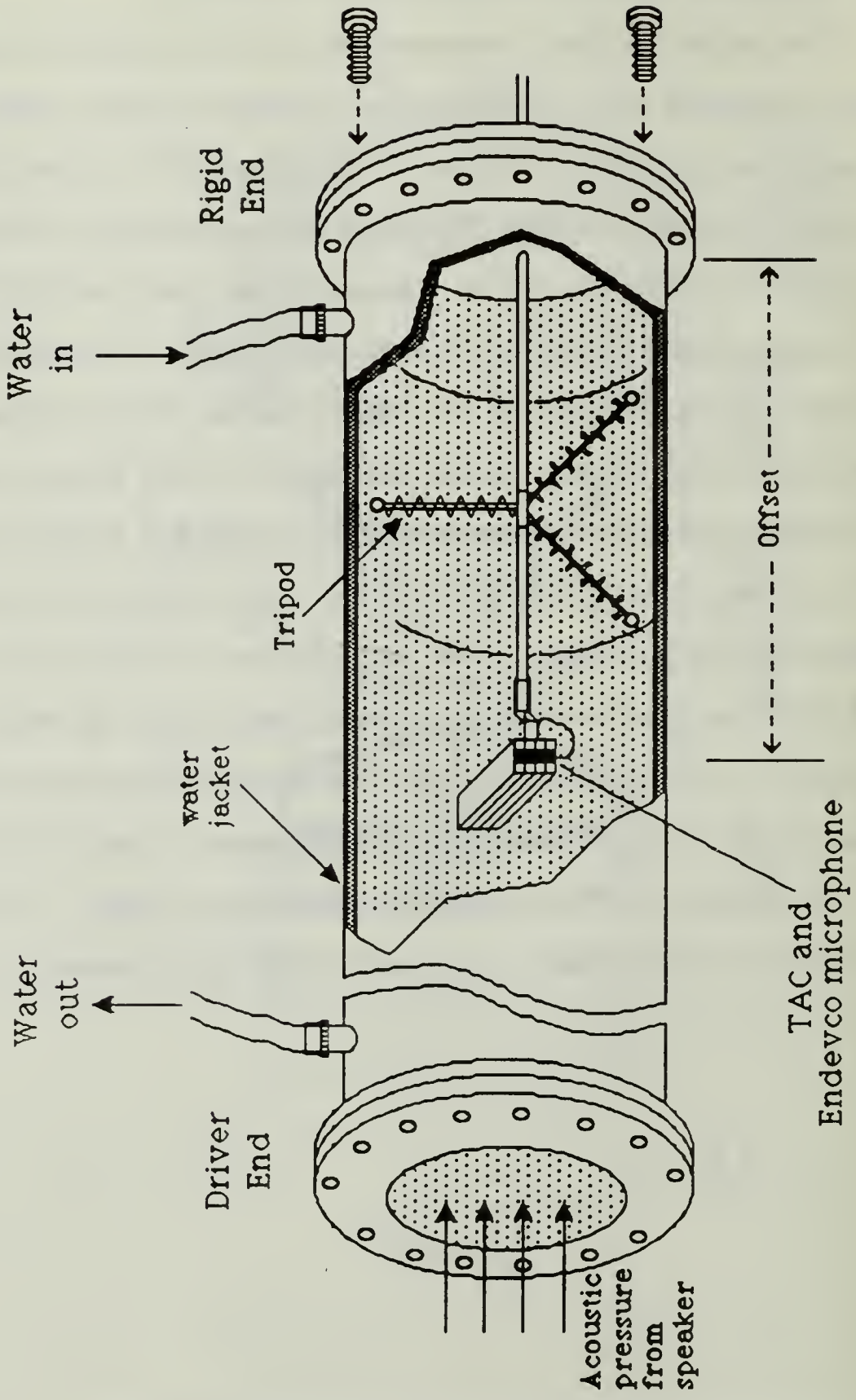

Fig. 13 The TAC and probe in the duct

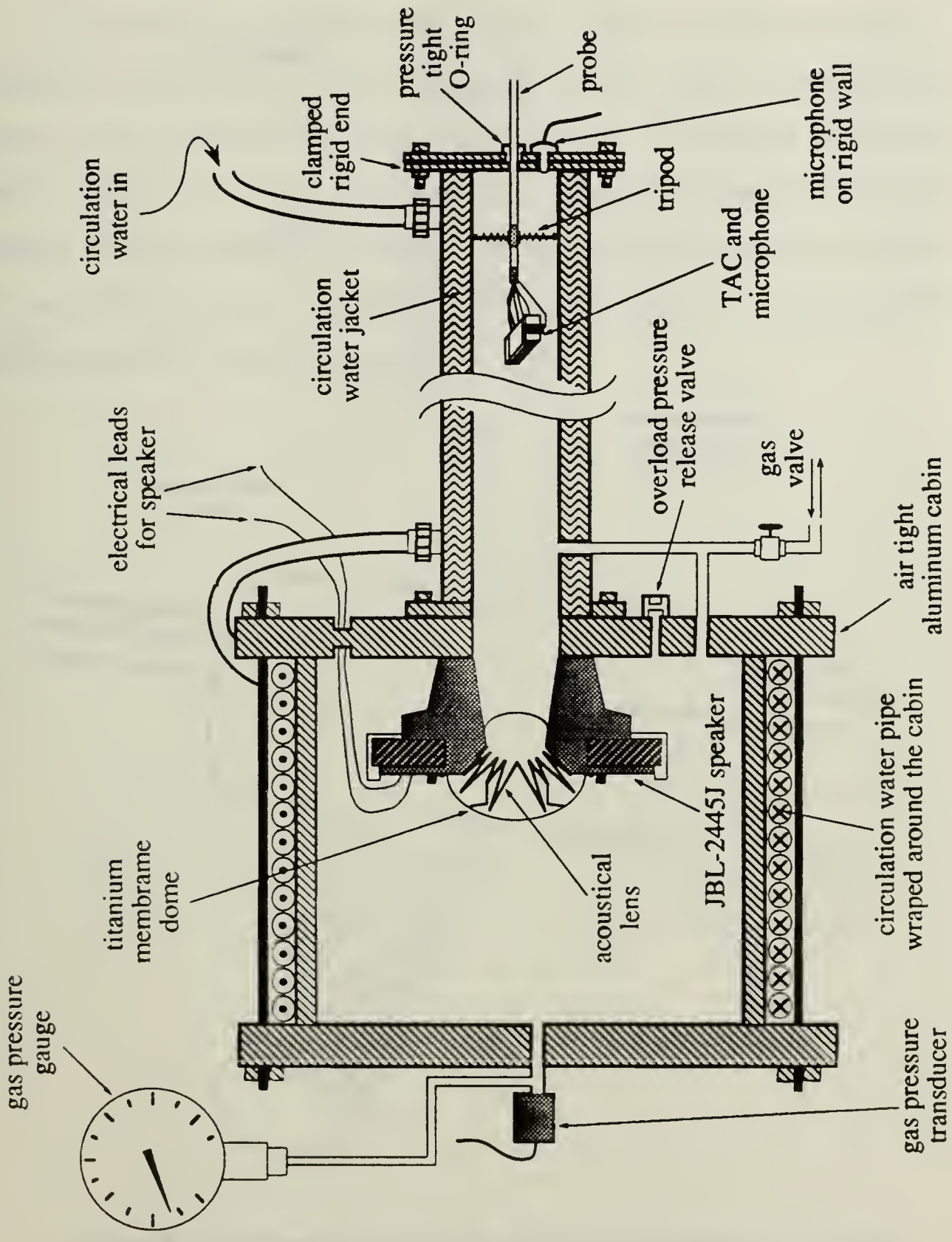

Fig. 14 The anatomy side view of the experiment setup

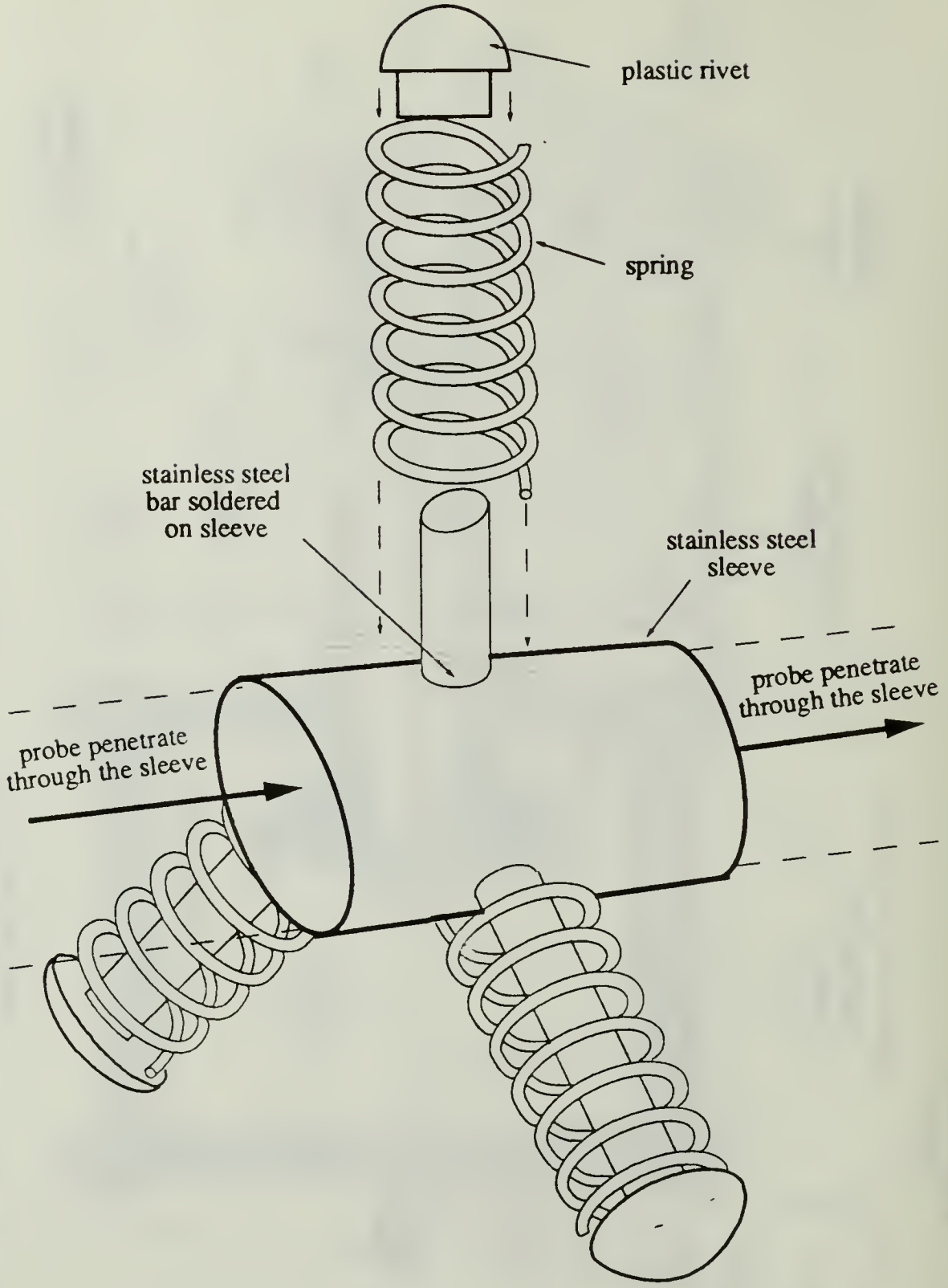

Fig. 15 The tripod fit for probe along with the duct inner diameter

4. TAC Positioning System

The TAC and probe are positioned within the resonator with a Compumotor Model M83-135 computer controlled stepper motor (25,000 steps/rev.) and a Compumotor Model 2100 indexer. The shaft of the stepper motor is connected to a lead screw, which in turn is connected to the probe through a traveling bracket. The motor, lead screw, and resonator are attached to an aluminum I-beam to provide rigidity and alignment. The integrated positioning system is depicted in Fig. 16.

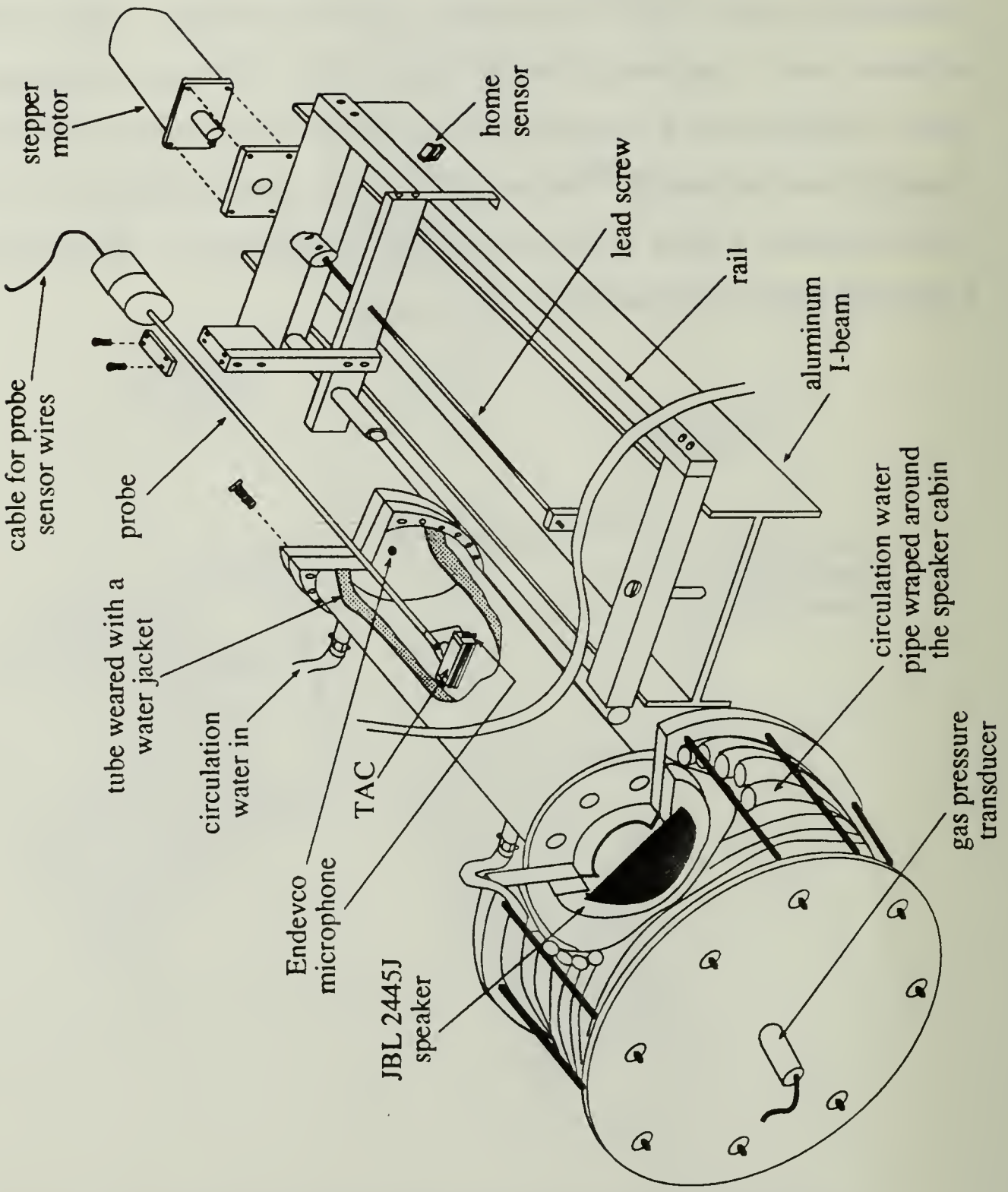

Fig. 16 The integration view of the experimental set up

5. Electronic Instrumentation

An instrument controlling and data acquisition program was written in QuickBASIC and was run by an IBM AT compatible computer. The function generator, the multimeter and the indexer were directly connected to the computer with GPIB cable individually. Through the program command execution, the function generator supplies the acoustic amplitude and frequency to the speaker; the indexer controls the movement of the stepper motor; and the multimeter collects all the data from the sensor terminals. An oscilloscope was used to monitor the source and output of the speaker. The signal analyzer was used to analyze the spectrum of the frequency distribution, through which a proper resonance frequency can be picked before the experiment is executed. The temperature reference for the multimeter was set up with an isothermal block, using a 4-wire method to measure the isothermal block temperature by means of a thermistor. The isothermal block is a common temperature reference base for the tube temperature and TAC. Fig. 17 is the block diagram of the electrical data acquisition system. The temperature reference and measurement circuits are shown in Fig. 18.

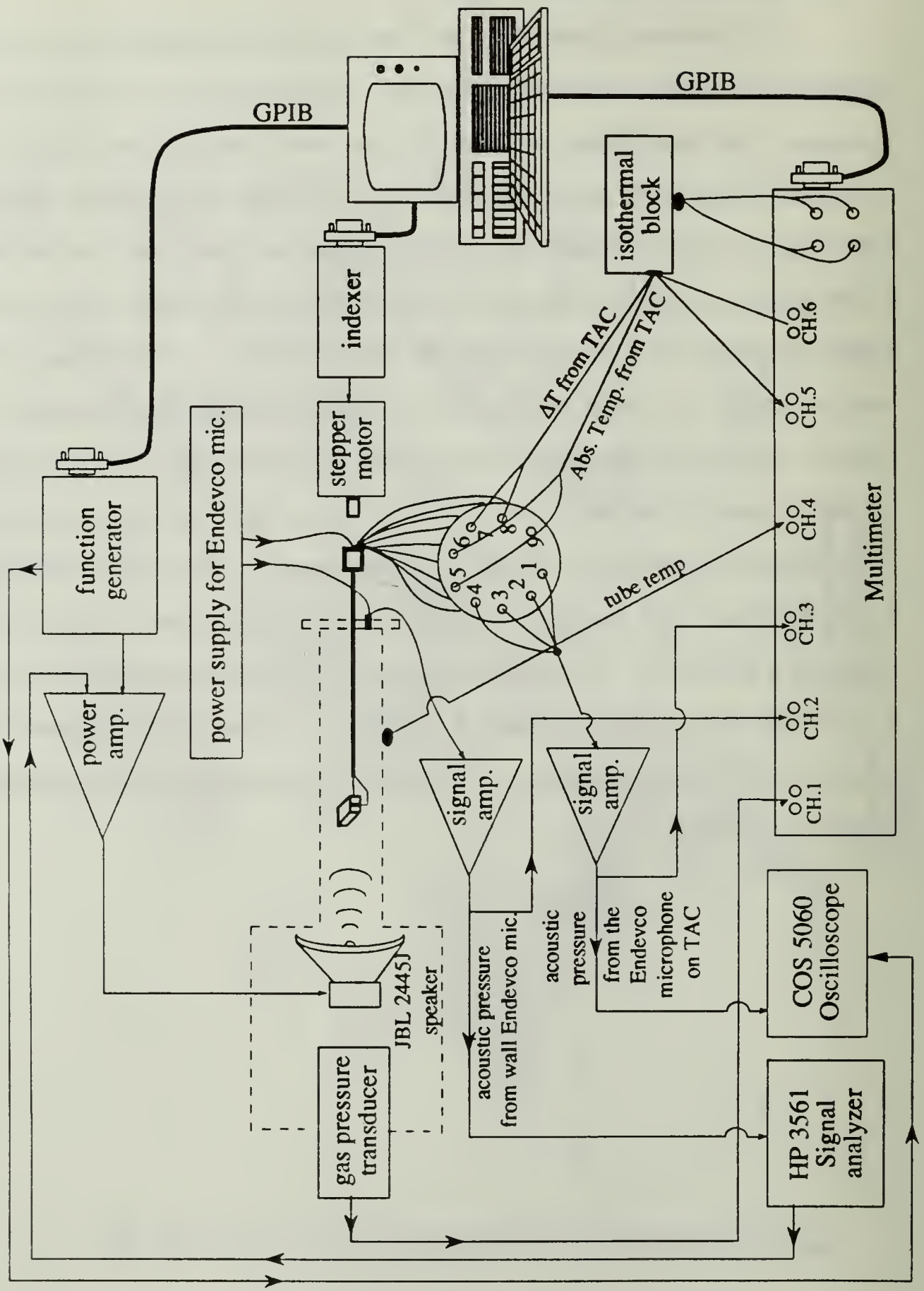

Fig. 17 The electrical data acquisition system

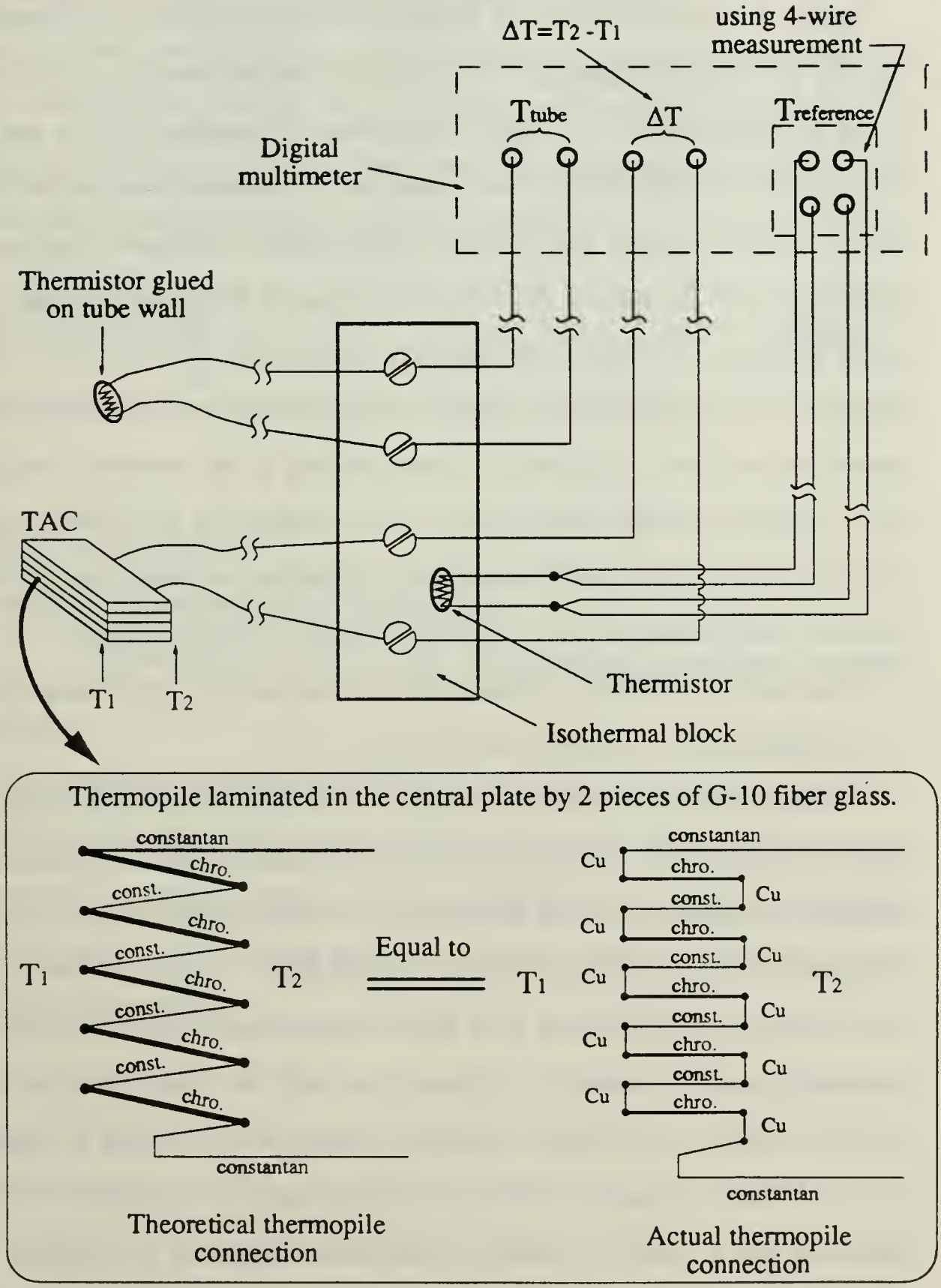

Fig. 18 The utilization of the TAC and temperature sensors in experiment system

C. EXPERIMENTAL PROCEDURE

Before the data acquisition is started, the water circulator was turned on and set with a constant temperature. For a series of experiments run with same type of gas and gas pressure, a constant environment temperature will be very helpful for the analysis of the results. The system will be pumped down and refilled with either Helium or Argon several times. Approximate resonance frequencies are determined next by driving the JBL-2445J speaker with the noise source of the signal analyzer. The rigid wall Endevco output then fed back into the signal analyzer. The displayed signal peaks among the frequency distribution spectrum denote the resonance frequencies corresponding to the resonant modes of the duct. The JBL speaker input source is now changed to the function generator which is set to individual resonance frequencies to check for interference between those resonances and higher harmonics of the driver signal.

The gain on the source voltage amplifier was set to a proper range according to the requirements of the drive ratio (P_{ac}/P_{gas}).

Automated data acquisition now starts. The program initially reads voltages from the gas pressure transducer and directly converts them to pressure. The reference temperature is then read directly from the multimeter and converted to a effective reference voltage through a polynomial. The low order polynomial was numerically determined from NBS Thermocouple Table over the limited temperature range of interest. Voltages from both the tube thermistor and TAC are read, added to the effective reference voltage, and converted to temperatures by an inverse polynomial. The driver voltage amplitude is set on the function generator and a search is made for resonance frequency by stepping on both sides of the previously determined natural frequency and reading the resultant

acoustic pressure amplitude. The frequency producing the highest acoustic pressure amplitude is selected and set in the function generator.

Once the preliminary readings are finished and the function generator set, the data run commences by reading the TAC output voltage and converting it to a temperature as discussed above. Then the TAC temperature difference (ΔT) will be converted from TAC output voltage as following:

$$\Delta T = \frac{V}{N}\frac{dT}{dV} = \frac{V}{N}\frac{1}{\frac{dV}{dT}} \qquad \text{Eq.(23)}$$

where

V = TAC output voltage

N = number of junctions in TAC thermopile

$\frac{dV}{dT}$ = the sensitivity of the type E (Chromel-Constantan junction) thermocouple

The TAC is then moved to the next position with 7 mm interval and a wait time of 45 seconds, activated and then readings are taken. The subsequent data runs were made at constant static pressure and increasing acoustic pressure by resetting the indexer to the home position and incrementing the driver voltage gain on the power amplifier.

IV. RESULTS AND DISUCSSION

A. INTRODUCTION

As described in the previous chapter, the data for this experiment consisted of measurements of the temperature difference across various TACs as a function of their position in the standing wave, the type of gas, the mean pressure of the gas, and the acoustic pressure amplitude. The results of these measurements are presented and discussed in this chapter.

B. RESULTS AND DISCUSSION

A typical experimental result for a low value of the drive ratio is presented in Fig. 19. Two curves are displayed on the graph. The dashed curve represents the magnitude of the acoustic pressure (in kPa) as measured with the microphone mounted next to the TAC as a function of the distance x of the center of the TAC from the closed end of the resonator. The value of the pressure magnitude is read using the right-hand ordinate. The solid curve represents the measured temperature difference across the TAC (in °C) also plotted as a function of x. The value of the temperature difference is read using the left-hand ordinate. In order to facilitate comparison with theory, however, we need to know how the temperature difference depends on the position of the TAC relative to the standing wave, rather than on the TAC's position relative to the closed end of the tube. In other words, we need the temperature difference as a function of kx rather than x.

Ideally, x = 0 m would coincide with the closed end of the tube and, therefore, a pressure antinode. However, if there is an error in measuring the initial distance from the center of the TAC to the closed end of the tube or if the acoustic impedance of the resonator departs from that of the ideal case, this coincidence may not occur. We have chosen to avoid such complications by assuming that the position of the pressure node nearest the closed end should correspond to $kx = \frac{\pi}{2}$. The assumed position of the pressure node is then $x_{node} = \frac{\pi}{2k} = \frac{c}{4f}$. Using the measured value of the frequency and the thermodynamic value of c, x_{node} can be calculated. This value is then used to calibrate the x measurements by forcing the measured position of the pressure node to equal x_{node}. There are two ways to estimate the position of the pressure node. The first is to measure the magnitude of the pressure as a function of x, as displayed in Fig. 19, and then locate the position of the minimum. However, due to electrical interference between the microphone and the TAC, we were unable to measure the acoustic pressure magnitude and the temperature difference simultaneously. Hence, in order to acquire both quantities two data runs would have to be made for each set of acoustic parameters. In many circumstances, two data runs were made and the position of the pressure node determined as just described. However, a second method proved to be just as accurate and more time efficient.

The temperature difference is proportional to the product of acoustic pressure and particle velocity. Hence, when either of these quantities is zero so is the temperature difference. Therefore, the second method of locating the position of the pressure node is to locate the position of the zero in temperature difference. Close examination of Fig. 19 shows that the pressure node and the zero in the temperature difference are not exactly coincident. They are separated by

approximately 4 mm. Part of this discrepancy can be attributed to the fact that the acoustic center of the microphone may not be located at the center of the TAC. In this case, determining of the position of the pressure node with the microphone is inaccurate. After all, what we really want to know is when the center of the TAC is at the pressure node, not when the microphone is at the pressure node. Also, any ambient temperature gradients (nonthermoacoustic in origin) would effect the position of the zero in temperature difference. As described in the previous chapter, the resonator was surrounded by a temperature controlled, circulating water jacket which tended to minimize, but not completely eliminate, ambient temperature gradients. In any case, the acoustic wavelength for the situation presented in Fig. 19 is 1.64 m, so even a 4 mm error amounts to only 0.2% of a wavelength. We concluded that the second method of locating the pressure node is just as satisfactory as the first. In the discussions to follow, we present measurements of the temperature difference as a function of kx rather than x. The product kx is formed by multiplying the "calibrated" x by $k = \frac{2\pi f}{c}$.

Figure 20 illustrates the comparison between the measured temperature difference (the solid curve) and the theoretical temperature difference (the dashed curved) for a drive ratio of 0.28%. The theoretical temperature difference is computed using Eq. (20). (The experimental parameters for this data set, as well as those for Figures 21, 22, and 23, are listed above the graph.) The temperature differences are plotted as functions of kx. The positions of the particle velocity and pressure antinodes are indicated on the graph. As seen in the figure, the overall comparison is good, though the measured temperature difference is approximately 20% larger than the predicted result. We attribute part of the discrepancy to an uncertainty in the thermal conductivity of the

materials used to construct the TAC. Also, as seen later, measurements taken with TACs of essentially the same design give slightly different results. In general, however, the measured and predicted results are in reasonably good agreement at low drive ratios.

Figure 21 illustrates the effect of increasing the drive ratio to 1.99%. Four areas for comparison are obvious. First, the agreement is quite good in the vicinity of the pressure antinode. The slopes of the measured (solid curve) and predicted (dashed curve) temperature differences are approximately equal. Secondly, the agreement in the vicinity of the velocity antinode is poor. The slope of the measured temperature difference is much less than that of the predicted result. Third, the data series of the measured temperature difference is quite irregular, and jagged in the vicinity of the maximum temperature difference. Finally, the measured maximum temperature difference is significantly less and occurs at a different position than the predicted maximum. In short, the agreement between theory and experiment is poor at high drive ratios except near the pressure antinode.

Figure 22 illustrates the theoretical temperature difference as a function of kx for drive ratios from 0.17 to 1.99%. (The individual values of the drive ratio have been omitted, in order to reduce clutter on the graph. The data presented in Figs. 20 and 21 are a subset of these data.) This graph clearly indicates the progression from a sinusoid to a sawtooth curve and the displacement of the maximum temperature difference toward the pressure antinode as described by Wheatley et al [Ref. 2]. The actual temperature differences are shown in Fig. 23 for the same experimental conditions. The measurements do confirm qualitatively the sinusoid-to-sawtooth progression. Notice the dashed curve demarcates two

regions of behavior. The curves between the kx axis and this curve are smooth and regular. The curves on the other side of the dashed curve become jagged and irregular. This transition occurs in all of the data sets we have taken.

In order to quantify the comparison of these two figures, three ratios will be examined. The first ratio is that of the experimental slope of the temperature difference curve in the vicinity of the velocity antinode to the theoretical slope in the vicinity of the velocity antinode. The second ratio is the ratio of the experimental to theoretical slope in the vicinity of the pressure antinode. The final ratio is that of the maximum experimental temperature difference to the maximum theoretical temperature difference. As seen in Fig. 23, the temperature difference reaches a maximum on both sides of the pressure antinode, so two values of the maximum temperature difference ratio can be computed. These ratios are plotted as functions of the drive ratio (in %) in Fig. 24 for the data presented in Figs. 22 and 23. The slope in the vicinity of the velocity antinode is labeled "SOVmax", while the slope in the vicinity of the pressure antinode is labeled "SOPmax". The maximum temperature difference ratio to the left of the pressure antinode is labeled "1st", while the one to the right is labeled "2nd".

All ratios have approximately the same value for drive ratios less than approximately 0.4%. The ratios then start to decrease in a more-or-less linear fashion for drive ratios between approximately 0.4 to 1.0%. At this point the quasilinear decrease stops. It should be pointed out that the data for the drive ratio of 1.03% correspond to the dashed curve in Fig. 23 which demarcates the regions of regular and irregular behavior. As the drive ratio increases beyond approximately 1.0%, the pressure antinode slope ratio increases slightly and then levels off at a drive ratio of approximately 1.5%. In the drive ratio region above

1.0%, the temperature difference ratio more-or-less levels off, whereas the velocity antinode slope ratio tends to decrease, though at a slower rate than in the 0.4 to 1.0% drive ratio region.

Graphs similar to that in Fig. 24 are presented for several data sets taken with TAC #3 in Figs. 25 through 27. (The type of gas and the approximate mean gas pressure is given above the graph. Also, since the two maximum temperature difference ratios exhibit approximately the same behavior, the second one has been omitted to reduce clutter.) Each of these figures exhibit the same general features as Fig. 24, most importantly, the initial values of approximately 1.2, the region of linear decrease for drive ratios up to approximately 1.0%, and the generally leveling off behavior beyond.

Data taken with TAC #1 in helium are presented in Fig. 28 and 29. Again, the same general behavior is evident. One noticeable difference is in the initial values of the slopes, which are approximately 0.9 for TAC #1. This change in initial value is consistent with our claim that much of the discrepancy between theory and measurement in Fig. 20 is due to variability between individual TACs and uncertainty in the value of the thermal conductivity of the TAC materials.

Data taken with TAC #2 are shown in Figs. 30 and 31. Although discussed in the previous chapter, TAC #2 and TAC #3 are much the same, there is some variability in the results obtained with the two TACs, as seen by comparing Figs. 24 and 30. The main differences are that the wires used for the thermopiles are different diameters. Although these data do not extend to high drive ratios, the same general behavior is observed as in Figs. 24 through 29. The initial values of the slopes are between approximately 1.0 and 1.1.

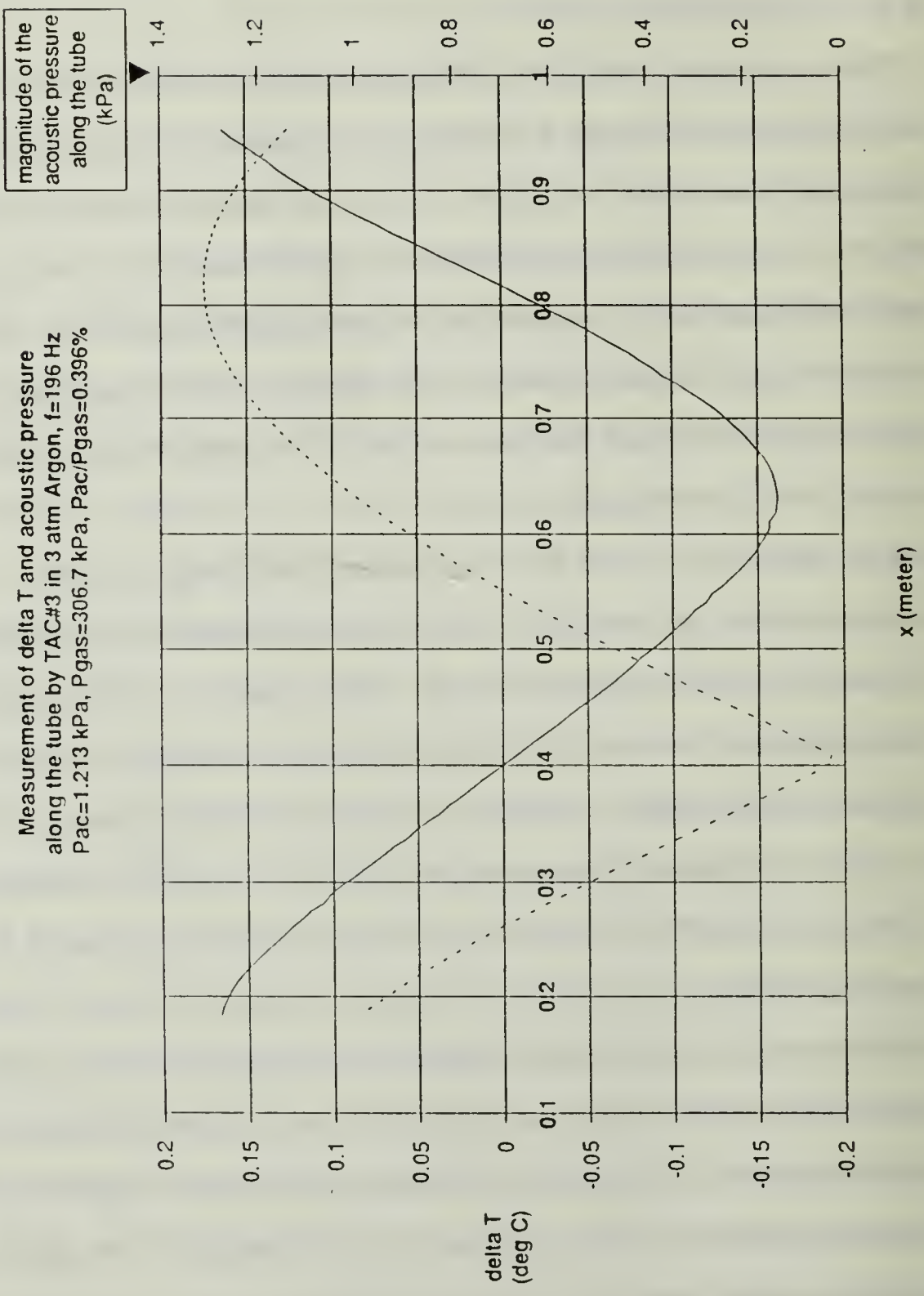
Measurement of delta T and acoustic pressure
along the tube by TAC#3 in 3 atm Argon, f=196 Hz
Pac=1.213 kPa, Pgas=306.7 kPa, Pac/Pgas=0.396%
magnitude of the acoustic pressure along the tube (kPa)
delta T (deg C)
x (meter)
0.2
0.15
0.1
0.05
0
-0.05
-0.1
-0.15
-0.2
1.4
1.2
1
0.8
0.6
0.4
0.2
0
0.1
0.2
0.3
0.4
0.5
0.6
0.7
0.8
0.9
1

Fig. 19

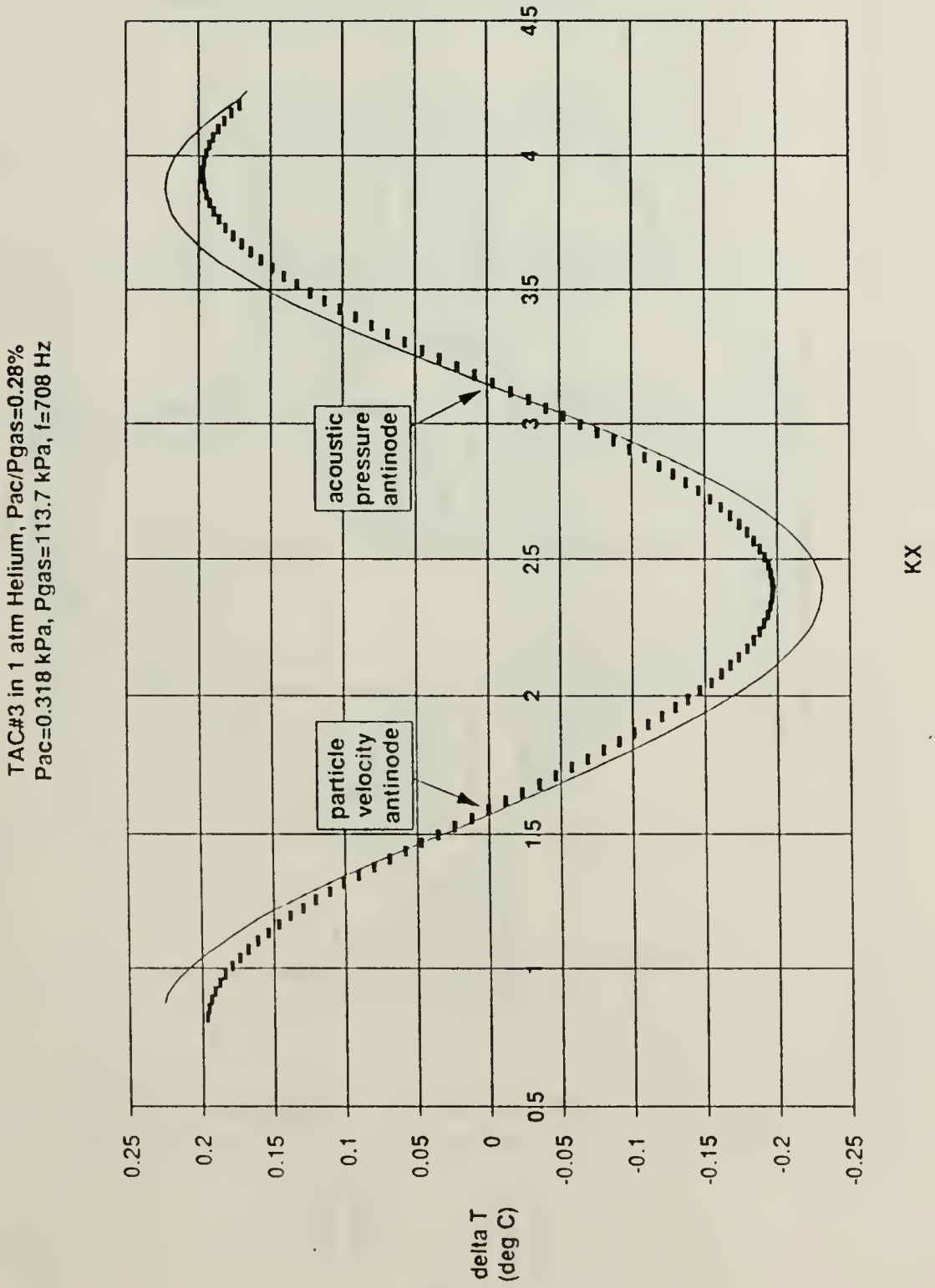
TAC#3 in 1 atm Helium, Pac/Pgas=0.28%
Pac=0.318 kPa, Pgas=113.7 kPa, f=708 Hz
acoustic pressure antinode
particle velocity antinode
delta T (deg C)
KX
0.25
0.2
0.15
0.1
0.05
0
-0.05
-0.1
-0.15
-0.2
-0.25
0.5
1
1.5
2
2.5
3
3.5
4
4.5

Fig. 20

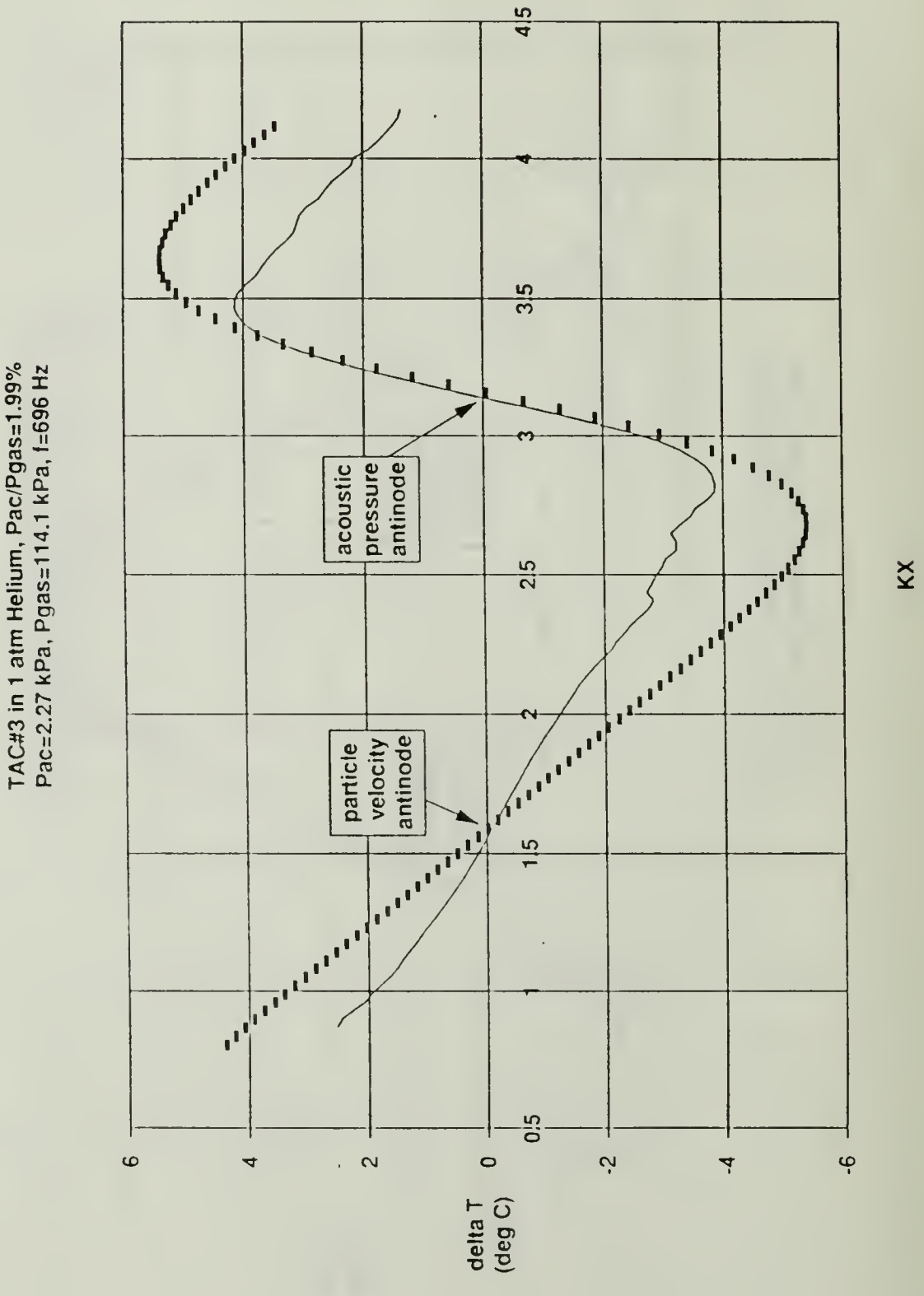
TAC#3 in 1 atm Helium, Pac/Pgas=1.99%
Pac=2.27 kPa, Pgas=114.1 kPa, f=696 Hz
acoustic pressure antinode
particle velocity antinode
delta T (deg C)
6
4
2
0
-2
-4
-6
0.5
1
1.5
2
2.5
3
3.5
4
4.5
KX

Fig. 21

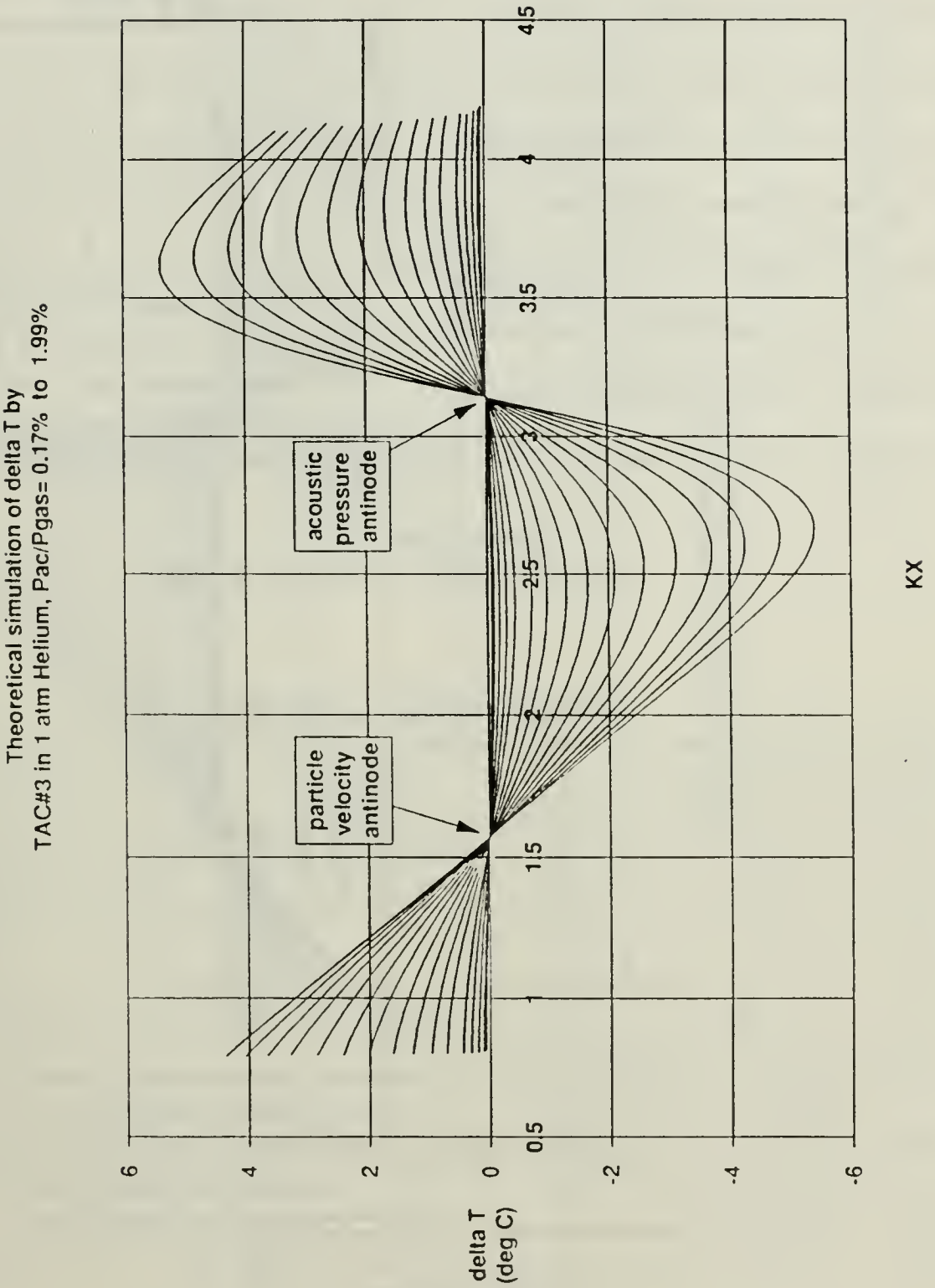
Theoretical simulation of delta T by
TAC#3 in 1 atm Helium, Pac/Pgas= 0.17% to 1.99%
acoustic pressure antinode
particle velocity antinode
delta T (deg C)
KX
6
4
2
0
-2
-4
-6
0.5
1
1.5
2
2.5
3
3.5
4
4.5

Fig. 22

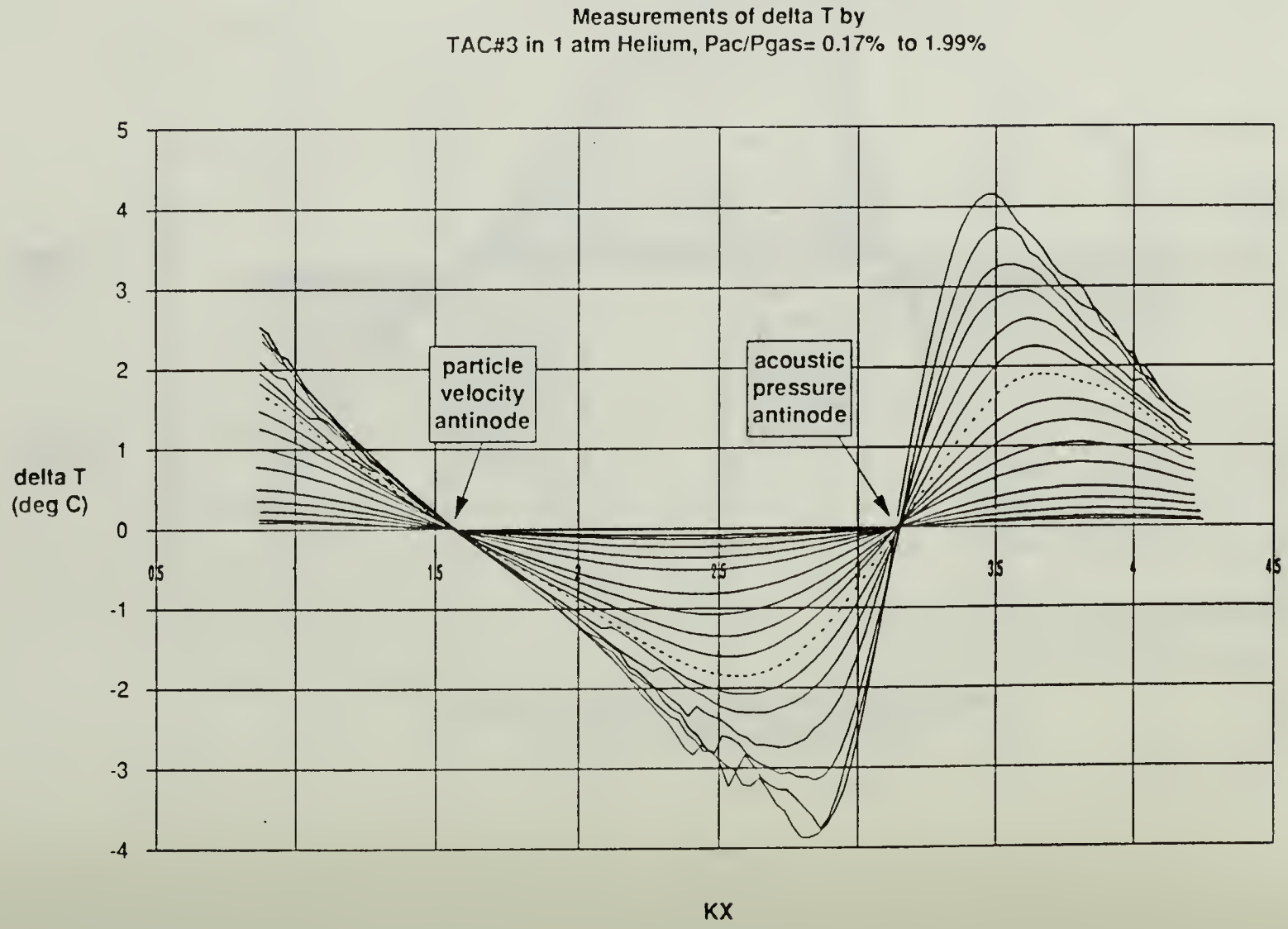
Measurements of delta T by
TAC#3 in 1 atm Helium, Pac/Pgas= 0.17% to 1.99%
delta T
(deg C)
KX
particle
velocity
antinode
acoustic
pressure
antinode
5
4
3
2
1
0
-1
-2
-3
-4
0.5
1.5
2.5
3.5
4.5

Fig. 23

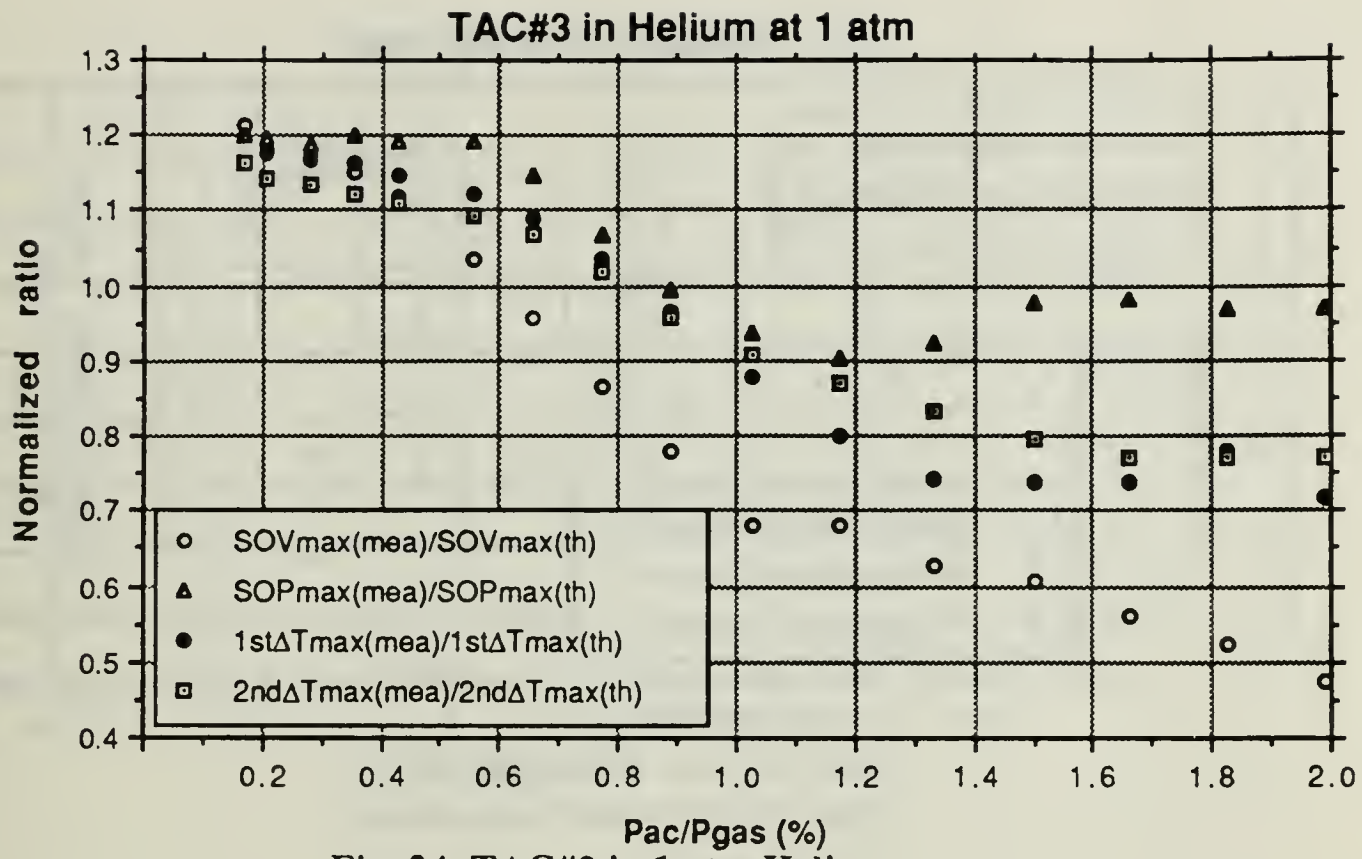

Fig. 24 TAC#3 in 1 atm Helium

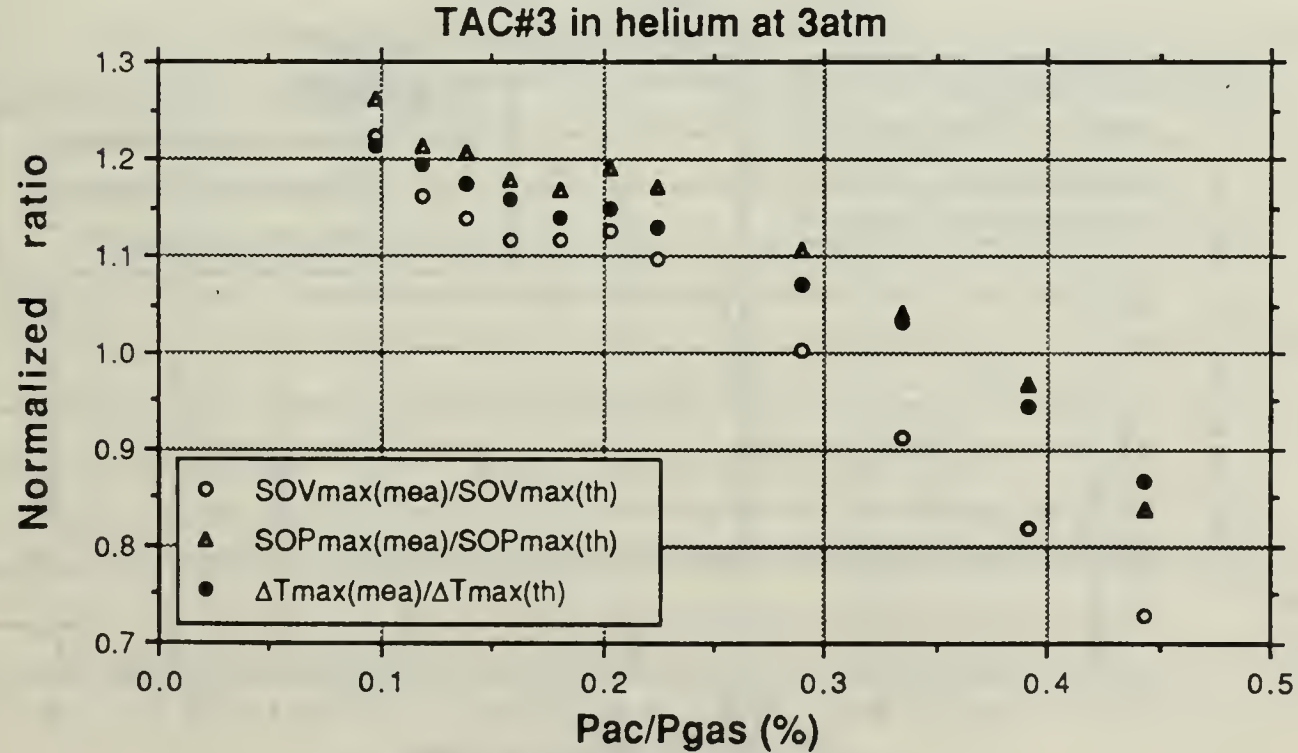

Fig. 25 TAC#3 in 3 atm Helium

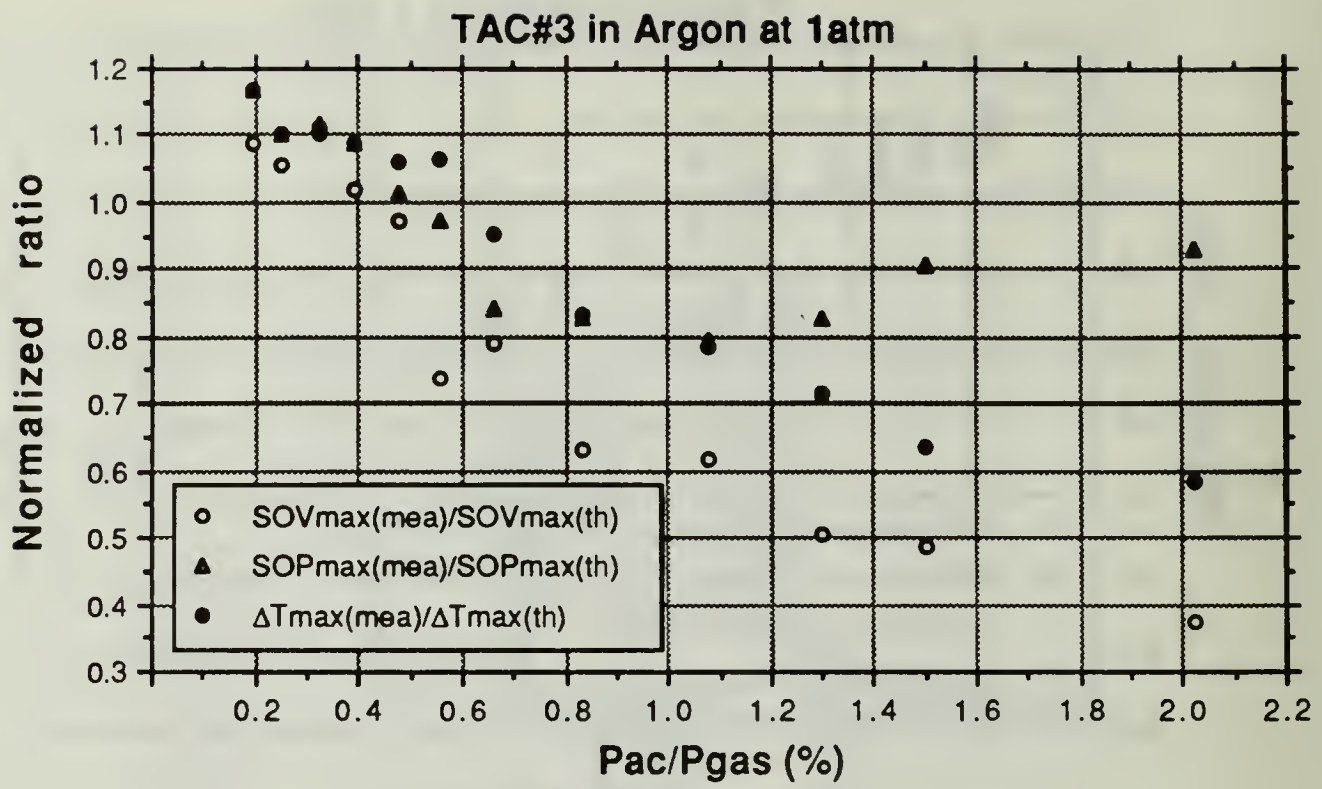

Fig. 26 TAC#3 in 1 atm Argon

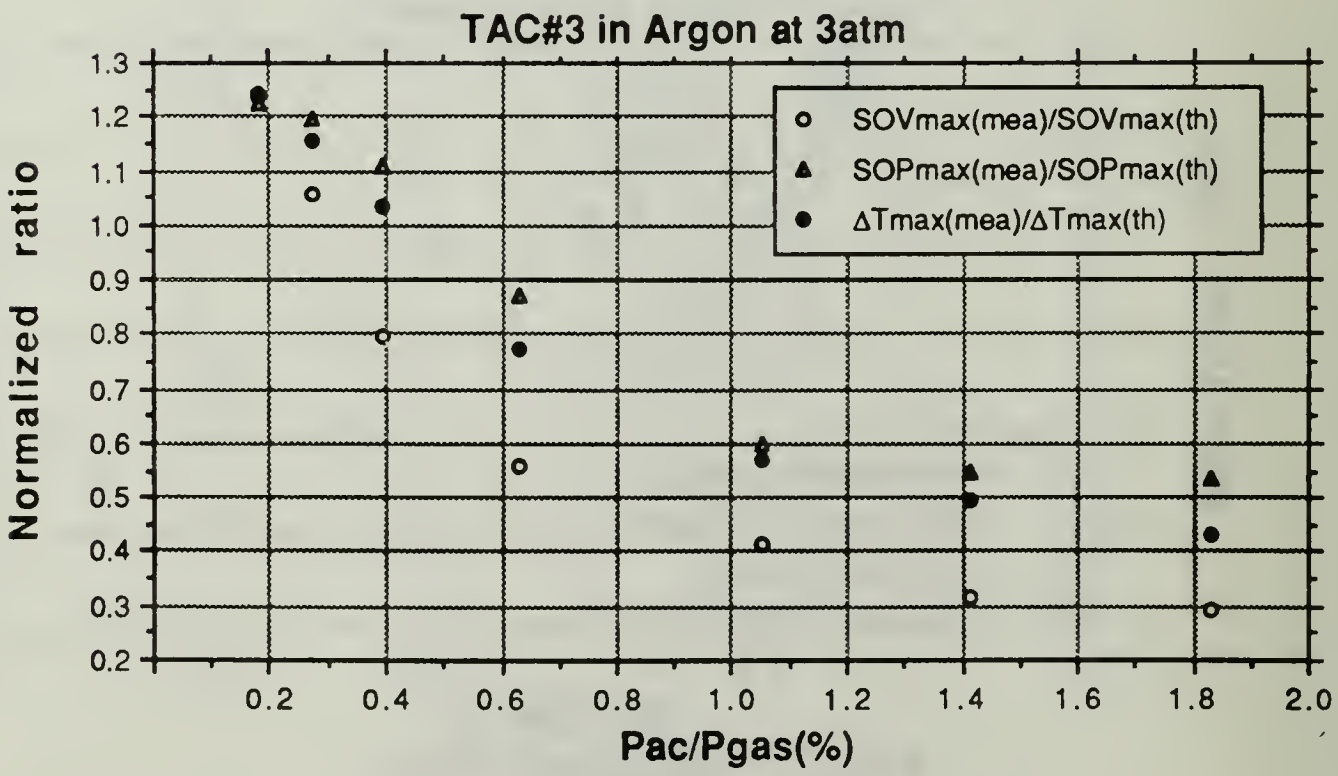

Fig. 27 TAC#3 in 3 atm Argon

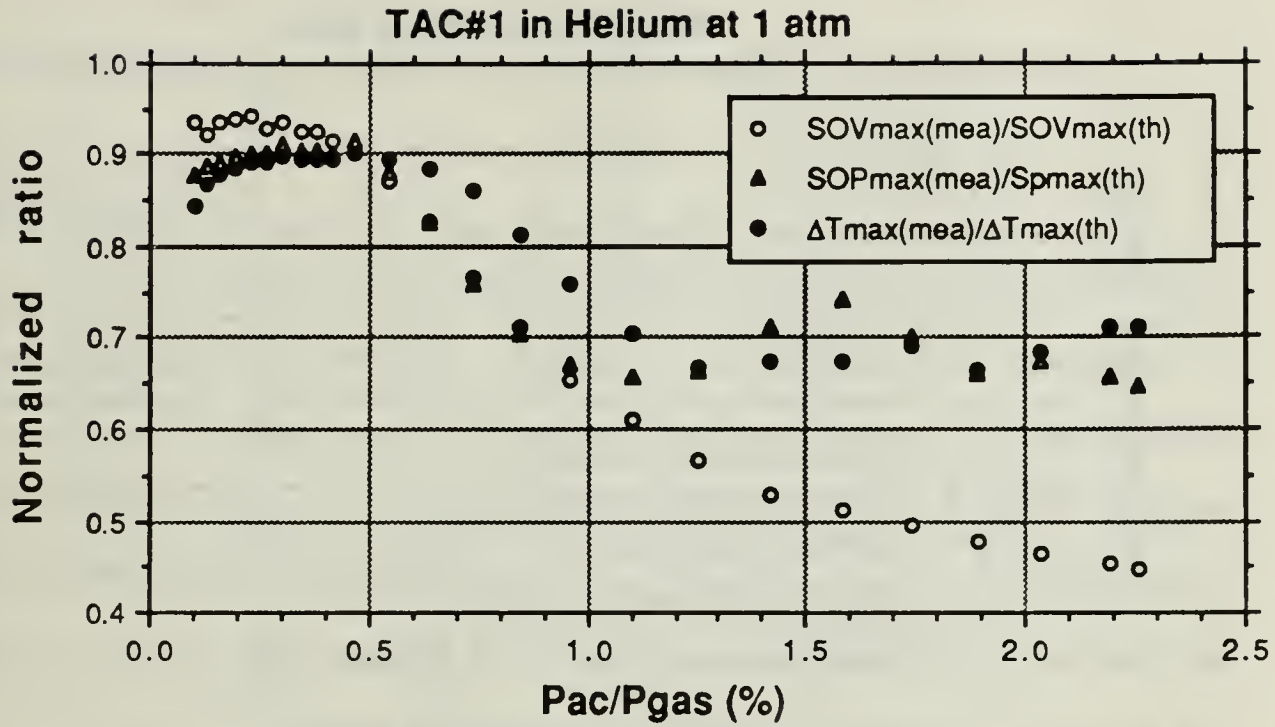

Fig. 28 TAC#1 in 1 atm Helium

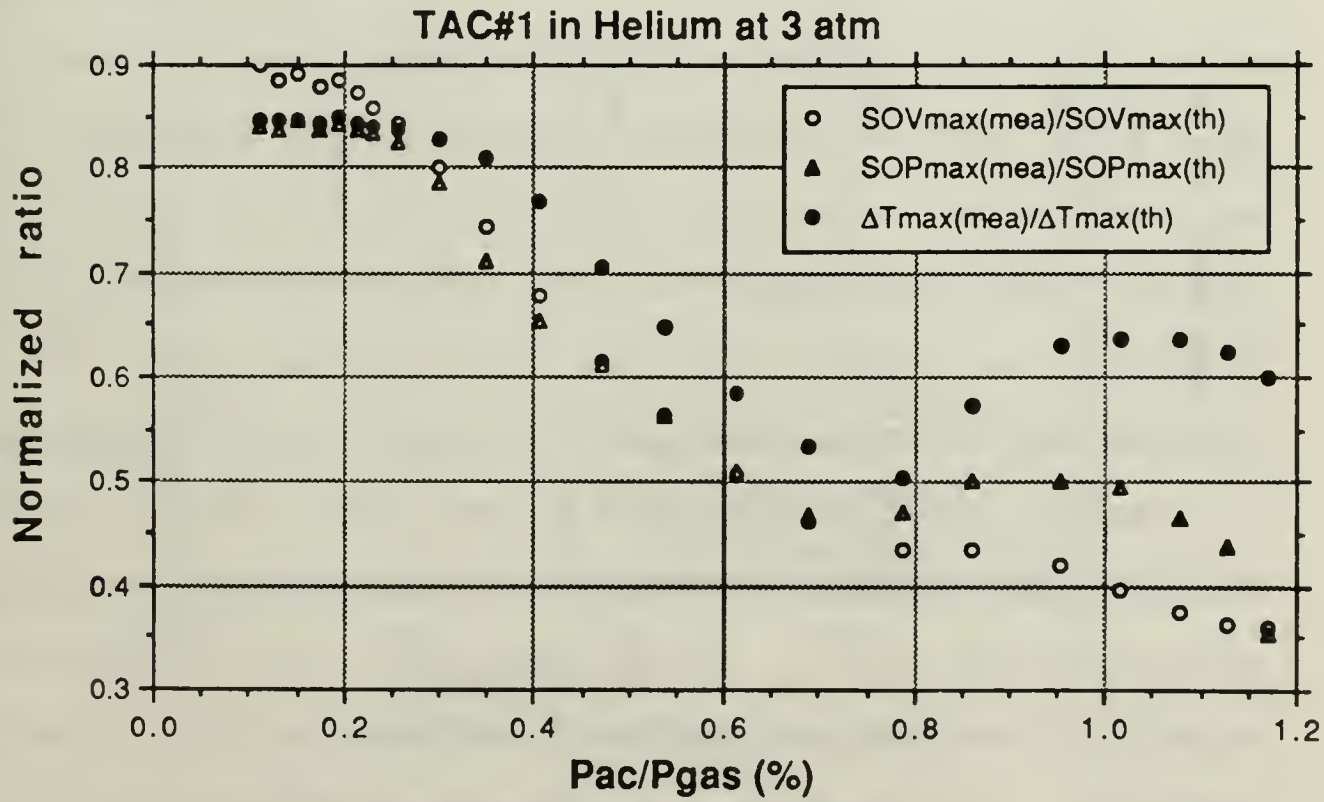

Fig. 29 TAC#1 in 3 atm Helium

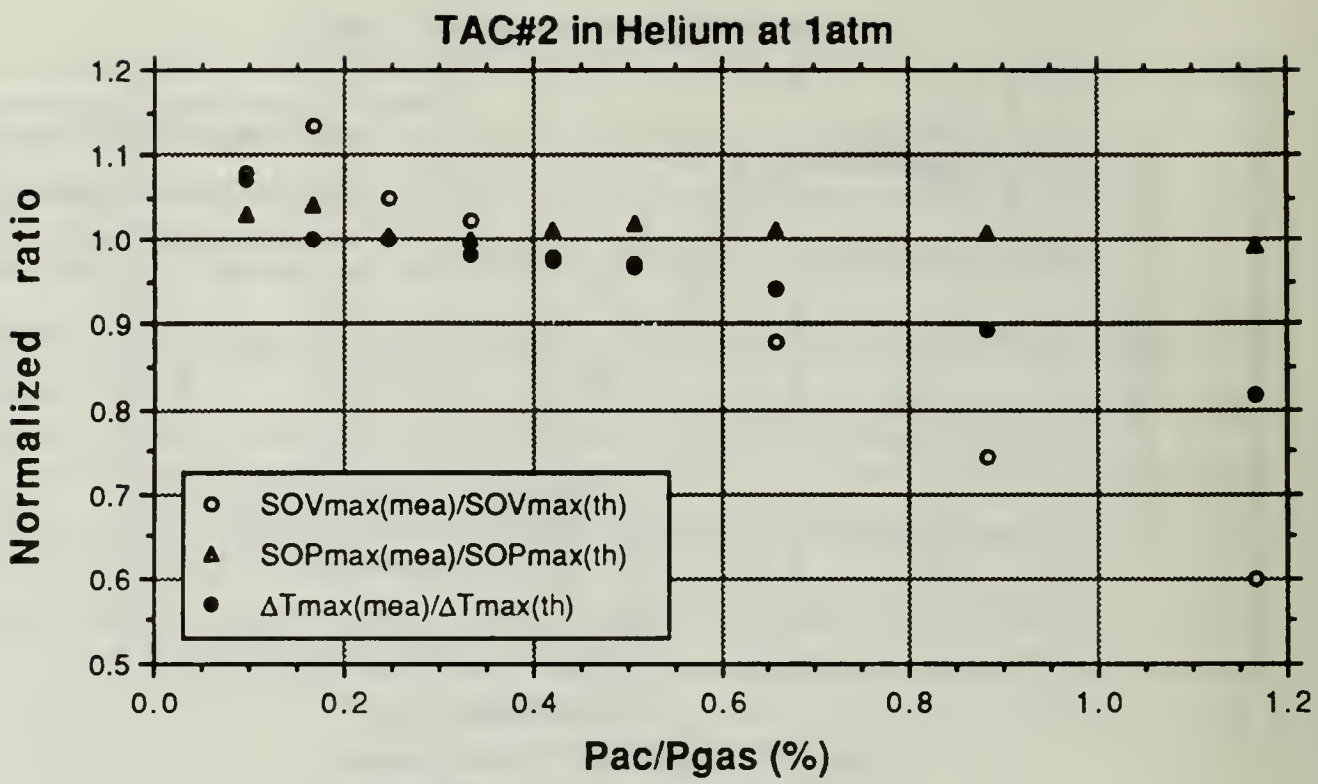

Fig. 30 TAC#2 in 1 atm Helium

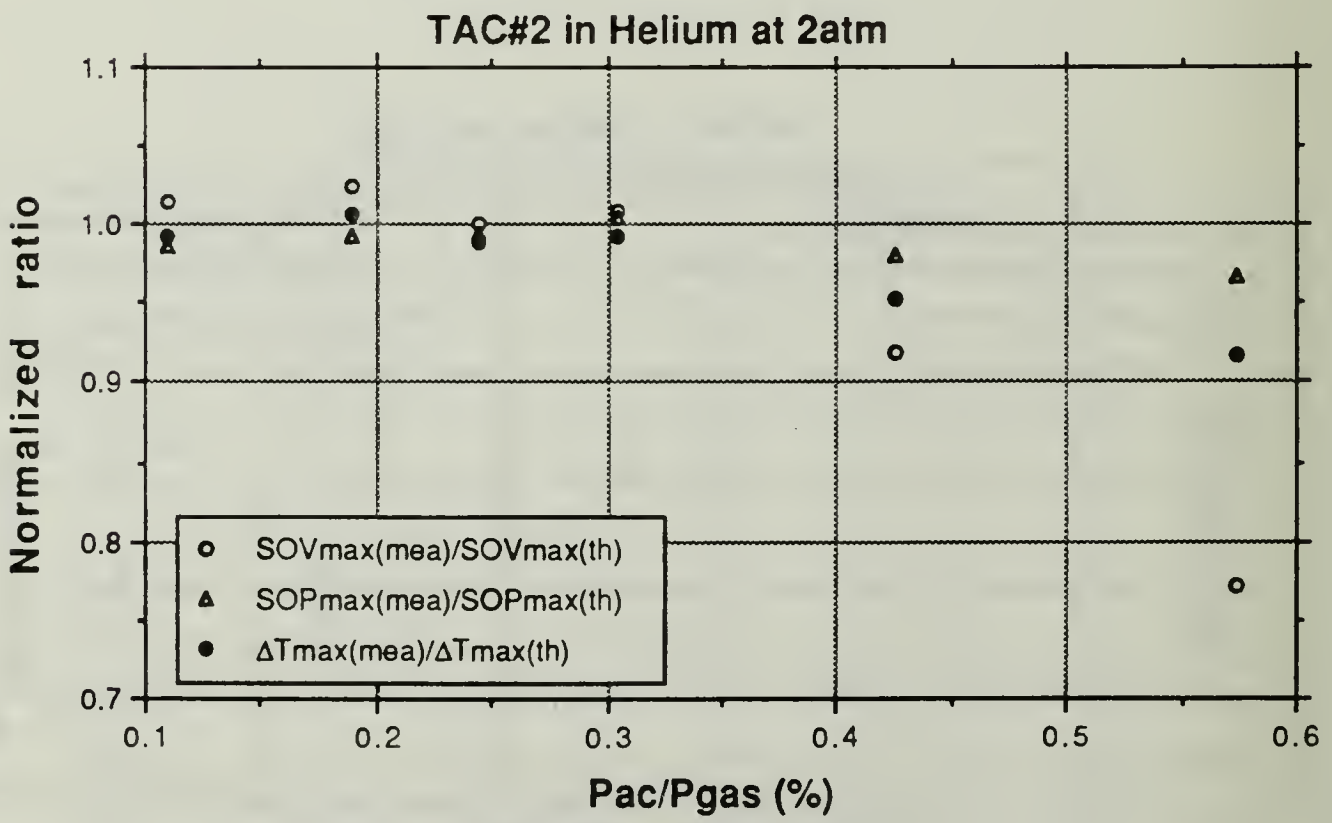

Fig. 31 TAC#2 in 2 atm Helium

V. SUMMARY, CONCLUSIONS, AND FUTURE WORK

A. SUMMARY

The goal of this thesis is to make a quantitative investigation of the basic theory underlying the thermoacoustic effect. The experimental approach has been to measure the temperature difference developed across a thermoacoustic couple (TAC) as a function of the position of the plates in an acoustic standing wave, the drive ratio, the thermal properties of the plates, and the thermophysical properties of the gas. The specific aim of these measurements is to first verify the theory developed by Wheatley et al by comparing it to measured results at low drive ratios, and, secondly, to extend the comparisons to high drive ratios. In order to make these measurements a computer controlled device has been designed and built.

The results of measurements made with three different TACs in helium and argon for mean gas pressures between approximately 100 and 300 kPa are reported. In general, results can be summarized as follows. At low values of the drive ratio (below approximately 0.4%) the measurements agree well with predictions. The data series of the temperature difference as a function of position, changes from a sinusoid to a sawtooth as predicted. As the drive ratio increases from 0.4% to approximately 1%, the agreement between measured and predicted results decreases almost linearly with increasing drive ratio. The data series continues to distort, yet remains smooth. At drive ratios greater than approximately 1%, the data series of the measured temperature difference becomes irregular and the linear dependence on drive ratio stops. At the highest

drive ratios, the ratio of the measured results to the predicted results is more or less independent of drive ratio, although some exceptions were found. Finally, measured values of the temperature difference agree very well in the vicinity of the pressure antinode regardless of drive ratio. On the other hand, they don't agree very well at velocity antinodes.

B. CONCLUSIONS

Several conclusion may be drawn from this work. The first conclusion is that the thermoacoustic effect is well understood at low values of the drive ratio. In addition, the theory developed by Wheatley et al [Ref. 2] agree well with measured results. The second conclusion is that there are two distinct regions of behavior at higher drive ratios. One region, which occurs for drive ratios less that approximately 1%, is characterized by a linear decrease in the agreement between theory and experiment. The second region, which occurs for drive ratios greater than approximately 1%, is characterized by the onset of irregularities in the temperature difference data series. Also the linear dependence of the disagreement disappears. Further, because the agreement is always good in the vicinity of the pressure antinode (velocity node), some velocity dependent effect may be the cause of the poor agreement at higher drive ratios. This conclusion is also supported by the observation of the sudden onset of irregularities in the temperature difference data series. A final conclusion is that there is variability between TACs, even between those of essentially the same design. This conclusion indicates that the experimental apparatus developed for these measurements may be useful in searching for an optimal TAC designs.

C. FUTURE WORK

One area for future work is to develop a method of measuring the thermal conductivity of the materials used to construct the TACs or calibrating the TAC once it is constructed. A calibration may be accomplished by imposing a known temperature difference across the TAC and measuring the output voltage. Though not discussed in this thesis, we have made a first attempt at calibrating TACs. The results were unsatisfactory in that they showed wide variability. We intend to pursue TAC calibration in the future. Once a TAC can be calibrated, we can investigate the causes of the variability in agreement between experiment and prediction at low drive ratios.

Another area for future work is to measure the acoustic particle velocity, most likely with hot wire anemometry. This capability will allow us to investigate the conclusion that velocity dependent effects, such as the onset of turbulence, are the cause of the disagreement between theory and experiment at high drive ratios.

Finally, we intend to use the experimental apparatus to investigate the behavior of thermoacoustic engines which are too long to be considered TACs, but which more closely resemble the type of engine used in refrigerators and heat pumps. It should be possible to not only investigate the design of the engine, but to investigate the optimum placement of the engine within the sound field.

LIST OF REFERENCES

1. John Wheatley, T. Hofler, G. W. Swift and A. Migliori, "*Experiments with an intrinsically irreversible acoustic heat engine*," Phys. Rev. Lett. 50, 499-502 (1983).

2. John Wheatley, T. Hofler, G. W. Swift and A. Migliori, "*An intrinsically irreversible thermoacoustic heat engine*," J. Acoust. Soc. Am. 74, 153-170 (1983).

3. John Wheatley, T. Hofler, G. W. Swift and A. Migliori, "*Understanding some simple phenomena in thermoacoustics with applications to acoustical heat engines*," Am. J. Phys. 53, 147-162 (1985).

4. G. W. Swift, A. Migliori, T. Hofler and John Wheatley, "*Theory and calculations for an intrinsically irreversible acoustic prime mover using liquid sodium as primary working fluid*," J. Acoust. Soc. Am. 78, 767-781 (1985).

5. A. Migliori and G. W. Swift, "*Liquid-sodium thermoacoustic engine*," Appl. Phys. Lett. 53, 355-357 (1988).

6. G. W. Swift, "*Thermoacoustic engines*," J. Acoust. Soc. Am. 84, 1145-1180 (1988).

7. McCarty R. D.,*Thermodynamical Properties of Helium-4 from 2-1500 K with Pressure to 1000 Atmosphere*, Washington D. C., NBS Technical Note 631, National Bureau of Standards, 1972

8. Muzzerall M. L., *Investigation of Thermodynamic Heat Transport Using A Thermoacoustic Couple*, Master's Thesis, Naval Postgraduate School, Monterey, California, 1987

9. Kite M. D., *Computerized Measurement of Thermoacoustically Generated Temperature Gradients*, Master's Thesis, Naval Postgraduate School, Monterey, California, 1988

10. *Thermal Conductivity Metallic Elements and Alloys*, published by IFI/Plenum Data Corporation 227 West 17th Street, New York NY.10011, copyrig© 1970, Purdue University

INITIAL DISTRIBUTION LIST

		No. of copies
1.	Library, Code 0142 Naval Postgraduate School Monterey, CA 93943-5002	2
2.	Professor A. Atchley, Code 61Ay Naval Postgraduate School Monterey, CA 93943	5
3.	Dr. T. J. Hofler, Code 61Hf Naval Postgraduate School Monterey, CA 93943	1
4.	Dr. G. W. Swift Condensed Matter & Thermal Physics (P-10) Los Alamos National Lab P.O. Box 1667/MS 764 Los Alamos, NM 87545	1
5.	Dr. Henrey E. Bass Physical Acoustics Research Laboratory University of Mississippi University, MS 38677	1
6.	Dr. L. E. Hargrove Physics Division, Code 1112 Office of Naval Research 800 N. Quincy Street Arlington, VA 22217	1
7.	Professor S. Garrett, Code 61Gx Naval Postgraduate School Monterey, CA 93943	1

No. of copies

8. Professor Lim, Hock — 1
Department of Physics
National University of Singapore
Kent Ridge, Singapore 0511
Republic of Singapore

9. F. M. Murray — 1
JBL Incorporated
8500 Balboa Blvd.
Northridge, CA 91329

10. LCDR M. D. Kite — 1
709 Bruce Court
Herndon, VA 22070

11. Captain Michael Muzzerall — 1
301 Daniel Place
Victoria, British Columbia
Canada V9C 1W2

12. Feng, Yen-chun — 1
7, Lane 72, Tsu-lin Rd.
Chin-tan, 23180
Sin-tien County, Taipei
Taiwan, R. O. C.

13. Ao, Chia-ning — 2
25 Woon-woo Street
Taichung, 40403
Taiwan, R. O. C.

14. Library of Chinese Naval Academy — 1
P.O. Box 8494
Tso-ying, Kaohsiung
Taiwan, R. O. C.

15. Library of Chung-cheng Institute of Technology — 1
Ta-shih, Tao-yuan
Taiwan, R. O. C.

		No. of copies
16.	Chung-san Institute of Science and Technology P.O. Box 1, Lung-tan, Tao-yuan Taiwan, R. O. C.	1
17.	Chung-wei, Chen SMC#1505 NPS Monterey, CA 93943-5000	1
18.	Hsing-Han, Meng SMC#2308 NPS Monterey, CA 93943-5000	1
19.	Kao, Chih-chung SMC#2094 NPS Monterey, CA 93943-5000	1
20.	Lu, Han-chung SMC#1610 NPS Monterey, CA 93943-5000	1
21.	Lin, Hsiao-tseng SMC#1081 NPS Monterey, CA 93943-5000	1
22.	Lt. Robert C. Dees, USN 207 Lauber Ln. Derby, KS 67037	1
23.	Defence Technical Information Center Cameron Station Alexandria, VA 22304-6145	2

Thesis
A5673 Ao
c.1 The measurements of thermoacoustic phenomena using thermoacoustic couples.

Thesis
A5673 Ao
c.1 The measurements of thermoacoustic phenomena using thermoacoustic couples.

The measurements of thermoacoustic pheno
3 2768 000 85633 0
DUDLEY KNOX LIBRARY